

Bayesian Transfer Operators in Reproducing Kernel Hilbert Spaces

Septimus Boshoff¹ , Sebastian Peitz² , Stefan Klus³ 

¹Paderborn University, Germany ²TU Dortmund, Germany ³Heriot-Watt University, UK

septimus.boshoff@uni-paderborn.de sebastian.peitz@tu-dortmund.de s.klus@hw.ac.uk

Keywords: sparse Gaussian processes, probabilistic regression, variational learning, dynamical systems, Koopman operator, data-driven discovery, dynamic mode decomposition

Abstract

The Koopman operator, as a linear representation of a nonlinear dynamical system, has been attracting attention in many fields of science. Recently, Koopman operator theory has been combined with another concept that is popular in data science: reproducing kernel Hilbert spaces. We follow this thread into Gaussian process methods, and illustrate how these methods can alleviate two pervasive problems with kernel-based Koopman algorithms. The first being sparsity: most kernel methods do not scale well and require an approximation to become practical. We show that not only can the computational demands be reduced, but also demonstrate improved resilience against sensor noise. The second problem involves hyperparameter optimization and dictionary learning to adapt the model to the dynamical system. In summary, the main contribution of this work is the unification of Gaussian process regression and dynamic mode decomposition.

1 Introduction

Modeling and forecasting the behavior of noisy, high-dimensional, and nonlinear systems remains an active area of research. Yet, the governing laws of these systems are often unknown or prohibitively expensive to simulate. With the proliferation of measurement sensors and the advent of efficient computational hardware, our modern world is abundant with multi-fidelity data that enables us to construct models directly from data without relying solely on first principles. Beyond merely generating predictions, it is also possible to extract interpretable spatio-temporal patterns and coherent structures from the data, thereby deepening our understanding and enhancing our analysis of complex dynamical systems.

Transfer operator theory and *reproducing kernel Hilbert spaces* (RKHSs) are popular approaches that result in analytically informative algorithms [Mauroy et al., 2020, Klus et al., 2016, Brunton et al., 2022, Rasmussen and Williams, 2006, Shawe-Taylor, 2004, Berline and Thomas-Agnan, 2011, Cressie, 1990, Hofmann et al., 2008, Schölkopf and Smola, 2002], while also contributing widely to practical applications [Budišić et al., 2012, Saitoh et al., 2016, Rowley et al., 2009, Susuki and Mezic, 2011, Susuki et al., 2011, Berger et al., 2015, Bruder et al., 2019, Netto and Mili, 2018]. Both Koopman operator and RKHS techniques frame their corresponding problems in a functional analytic setting. Therefore, it stands to reason that by combining methods from both of these two fields, we can design robust algorithms that provide compact and interpretable models for (stochastic) time-series.

1.1 Dynamic Mode Decomposition

Transfer operators, such as the *Koopman* and *Perron-Frobenius operators*, describe the theory of linearizing a dynamical system, not merely around its fixed points, but globally without any approximation. The operator-theoretic perspective is particularly appealing because it is integrated with well-understood statistical and geometric perspectives, which ties in with insights into the physical behavior of dynamical systems [Mezic, 2019, Koopman, 1931, Koopman and Neumann, 1932].

The Koopman operator, being an infinite-dimensional object, must often be empirically approximated before it can be implemented on a computer. This involves discretizing the operator and identifying a suitable set of basis functions that span a finite-dimensional subspace wherein the spectral properties of the operator can be represented — a task that falls under the heading of *dictionary learning* [Li et al., 2017, Takeishi et al., 2017, Wehmeyer and Noé, 2018, Yeung et al., 2019, Azencot et al., 2020, Eivazi et al., 2021, Mardt et al., 2018].

One such suite of algorithms that discretizes the Koopman operator is *dynamic mode decomposition* (DMD; Schmid [2010], Williams et al. [2015a], Colbrook [2024]). DMD can be described as a Galerkin method that blends together *principal component analysis* (PCA) and the *discrete-time Fourier transform* [Colbrook and Townsend, 2024]. In other words, one may think of DMD as rotating the (lower) dimensional PCA space such that each basis has dynamics oscillating according to a single frequency and a single growth (or decay) rate.

In part, DMD remains attractive because it is based on an eigenvalue decomposition of a model obtained through linear regression. After projecting the system to a higher-dimensional space, DMD can provide accurate models of nonlinear [Williams et al., 2015a,b] and stochastic systems [Klus et al., 2020a, Wanner and Mezic, 2022, Črnjarić-Žic et al., 2020, Colbrook et al., 2024]. In other words, all the techniques belonging to linear time-invariant ODEs, such as spectral analysis, multi-step forecasting, numerical simulation, and even control [Peitz and Klus, 2019, Peitz et al., 2020, Proctor et al., 2016, Otto and Rowley, 2021] can be readily transferred to nonlinear systems. Moreover, should the system contain a large number of variables (e.g., in fluid dynamics), DMD can facilitate dimensionality reduction.

1.2 Gaussian Process Regression

Following the authors Williams et al. [2015b], Klus et al. [2018], DeGennaro and Urban [2019], Fujii and Kawahara [2019], Das and Giannakis [2020], Das et al. [2021], Ikeda et al. [2022], Bevanda et al. [2024], Klus et al. [2020b], Baddoo et al. [2022], Bevanda et al. [2025], the underlying machinery of our DMD algorithm is a reproducing kernel function (i.e., a covariance function). Kernel methods are *non-parametric*, enhance interpretability of features, and are generally more flexible compared to parametric models (e.g., multilayer perceptrons), since they encompass *all* functions sharing the same degree of smoothness. It is the non-parametric nature of kernel algorithms that grant them the intrinsic ability to implicitly construct a functional basis for a model directly from data. Thereby, they provide a natural choice for the hypotheses space: an RKHS. It is these properties that often lead to strong theoretical performance guarantees [Schölkopf and Smola, 2002, Klus et al., 2020c, Philipp et al., 2024].

One popular kernel regression framework (for modeling dynamical systems), is *Gaussian process (GP) regression* [Rasmussen and Williams, 2006, MacKay et al., 1998, Girard et al., 2002a, Wang et al., 2005, Solak et al., 2002]. GP regression is a function approximation technique that is capable of providing accurate estimations of an unknown function based on a limited set of noisy training targets and high-level assumptions about the function. Moreover, a GP model is numerically straightforward to estimate, the predictions of the model are fully probabilistic, and the theory provides a well-founded framework for model selection.

1.3 Contributions of this work

The core idea is to transfer the attractive features of GP regression to DMD. Thereby, we develop a Bayesian interpretation of the *embedded Perron–Frobenius operator* [Klus et al., 2020b] which opens up avenues to extend kernel-based DMD algorithms with established sparsity and hyperparameter tuning techniques. The result is a modification of ‘Extended DMD’ (EDMD; Williams et al. [2015a]) that constructs models from *noisy* measurement data of a nonlinear dynamical system and provides uncertainty estimates for multi-step predictions.

The remainder of this paper is structured as follows. Section 2 introduces a Bayesian formulation of DMD, and Section 3 explores its mathematical consequences and numerical performance. Lastly, in Section 4, we conclude with some final remarks, open questions, and point toward straightforward extensions. In Appendix A we review (sparse) GP regression and the notation of Rasmussen and Williams [2006], and for convenience and completeness we also present an overview of (kernel) transfer operators [Klus et al., 2020b] in Appendix B.

2 Gaussian Process Dynamic Mode Decomposition

Because kernel-based DMD algorithms often quickly become impractical for large data sets due to the high training cost, one of our goals is to apply the variational free energy (VFE) method [Titsias, 2009] to kernel Koopman operators [Klus et al., 2020b]. For example, in Klus et al. [2020b], to estimate the Koopman matrix we need to take the inverse of a Gramian which has a complexity of $\mathcal{O}(N^3)$, where N is the number of training samples; moreover, the eigenvalue decomposition also has a complexity of $\mathcal{O}(N^3)$. Therefore, we are motivated to find a better trade-off between the model’s generalization error

and its computational complexity. We want a non-parametric model that automatically adapts to the complexity of the dynamics, but not to the point where all the training inputs define the basis dictionary.

We will demonstrate how our algorithm is a special case of EDMD [Williams et al., 2015a]. Which means that it inherits some of EDMD’s limitations [Colbrook et al., 2019, Colbrook and Townsend, 2025, Colbrook et al., 2023]. This should not be surprising, since it is quite common to derive the same expressions within either a frequentist or Bayesian framework. This duality between ridge-regression and Bayesian models is well-known, and has been pointed out in Rasmussen and Williams [2006], Hastie [2009], Poggio and Girosi [1990], Wahba [1990]. One might then assume that the choice of framework merely reflects an attitude, with each attitude corresponding to a preferred mode of reasoning about how to construct a (data-driven) model. However, we could argue that attitudes matter because they suggest different approaches to improving upon the state-of-the-art. Hence, one of our goals is to shed some light on this debate.

For example, EDMD does not intrinsically provide an optimization scheme for selecting either the hyperparameters or the dictionary, and therefore requires another explicit strategy, e.g., [Tabish et al., 2025]. Neither does EDMD provide uncertainty-aware predictions, nor does it take into account measurement noise from the outset. Our amalgamation of DMD and GP regression wraps up the entire model inference pipeline into one coherent theory that simultaneously addresses hyperparameter optimization and sparse dictionary learning. This naturally raises the question of whether such an approach is overly restrictive and sacrifices the flexibility of frequentist methods.

2.1 Operators as Random Variables

We start with a full Bayesian treatment of the *embedded* Perron–Frobenius operator (PFO) [Klus et al., 2020b], which we denote by $\mathcal{P}_\varepsilon : \mathbb{H} \rightarrow \mathbb{H}$. The embedded Perron–Frobenius operator, is the adjoint of the kernel Koopman operator. Unlike the PFO which propagates densities, the embedded PFO can be thought of as a push-forward map that acts on *representations* of probability densities. In short, the idea of feature maps is extended to the space of probability distributions by thinking of $\varphi(\mathbf{x}) \forall \mathbf{x} \in \mathbb{X}$ as an injective representation of a density function. See Appendix C for a more detailed discussion of kernel mean embeddings.

Let us consider the ‘implicitly’ lifted training data set obtained from a dynamical system as $(\Phi_X, \Phi_Y) = \{(\varphi(\mathbf{x}_i), \varphi(\mathbf{y}_i))\}_{i=1}^N$, where the targets $\{\mathbf{y}_i\}_{i=1}^N$ are produced by the discrete-time flow map $\mathbf{F} : \mathbb{X} \rightarrow \mathbb{X}$, and $\mathbb{X} \subseteq \mathbb{R}^D$. We further assume only *isotropic* measurement noise:

$$Y_i = \mathbf{F}(X_i) + \epsilon_i, \quad \text{where } \epsilon_i \sim \mathcal{N}^D(\mathbf{0}, \sigma_Y^2 \mathbf{I}_D).$$

In Appendix A, we reviewed Gaussian process regression with outputs in \mathbb{R} . We now extend this setting by taking the target space to be the RKHS \mathbb{H} . This presents a challenge of handling not just finitely many outputs, but an infinite number of output channels. To address this, we employ an *operator-valued* kernel, and subsequently derive the posterior GP associated with the embedded PFO.

For the sake of clarity, allow a brief oversimplification and consider the $D = 1$ case. In this setting, the feature map $\varphi(\mathbf{x}) := \kappa_{\text{pr}}(\mathbf{x}, \cdot) \in \mathbb{H}$ is defined by the GP *prior* over a one-dimensional flow map, i.e. a real- and scalar-valued kernel $\kappa_{\text{pr}} : \mathbb{X} \times \mathbb{X} \rightarrow \mathbb{R}$.

Definition 2.1. *Lifted Observation Model.* We assume that a noisy lifted target $\varphi(\mathbf{y}) \in \mathbb{H}$ can be approximated by the sum of the latent noise-free evaluation $\mu_{Y|\mathbf{x}} := \mathcal{P}_\varepsilon \varphi(\mathbf{x}) \in \mathbb{H}$ and zero mean Gaussian process noise:

$$\varphi(Y_i) \approx \mathcal{P}_\varepsilon \varphi(X_i) + \nu_i,$$

where $\nu_i(\mathbf{x}) \sim \mathcal{GP}(0, \sigma_Y^2 \kappa_{\text{bc}}(\mathbf{x}, \mathbf{x}'))$ models noise in the (infinite-dimensional) RKHS \mathbb{H} .

Table 1: *Nomenclature.* The symbols for some of the explicit and implicit data structures.

Variable	Symbol
Pseudo-inputs	$\mathbf{Z} := [\mathbf{z}_1, \dots, \mathbf{z}_M]$
Snapshot matrices	$\mathbf{X} := [\mathbf{x}_1, \dots, \mathbf{x}_N]$ $\mathbf{Y} := [\mathbf{y}_1, \dots, \mathbf{y}_N]$
Dictionaries	$\Phi_Z := [\varphi(\mathbf{z}_1), \dots, \varphi(\mathbf{z}_M)]$ $\Phi_X := [\varphi(\mathbf{x}_1), \dots, \varphi(\mathbf{x}_N)]$
Covariance functions	$\kappa_{\text{pr}}(\mathbf{x}, \mathbf{x}') := \langle \varphi(\mathbf{x}), \varphi(\mathbf{x}') \rangle_{\mathbb{H}}$ $\xi_{\text{pst}}(\mathbf{x}, \mathbf{x}') = \kappa_{\text{pst}}(\mathbf{x}, \mathbf{x}') \mathcal{C}_{\text{bc}}$
Covariance matrices	$\mathbf{K}_{ZZ} := \kappa_{\text{pr}}(\mathbf{Z}, \mathbf{Z})$ $\mathbf{K}_{ZX} := \kappa_{\text{pr}}(\mathbf{Z}, \mathbf{X})$
Covariance operators	$\Xi_{XX} := \kappa_{\text{pr}}(\mathbf{X}, \mathbf{X}) \otimes \mathcal{C}_{\text{bc}}$ $\hat{\mathbf{C}}_{XY} := (1/N) \Phi_X \Phi_Y^\top$
Feature vectors	$\mathbf{k}_Z(\mathbf{x}) := \Phi_Z^\top \varphi(\mathbf{x})$ $\xi_X(\mathbf{x}) := \mathbf{k}_X(\mathbf{x}) \otimes \mathcal{C}_{\text{bc}}$
Gramian matrix	$\mathbf{C}_{XX} := \mathbf{K}_{ZX} \mathbf{K}_{ZX}^\top$
Stiffness matrix	$\mathbf{C}_{XY} := \mathbf{K}_{ZX} \mathbf{K}_{ZY}^\top$
Regularization	$\hat{\mathbf{K}}_{XX} := \mathbf{K}_{XX} + \sigma_Y^2 \mathbf{I}_N$ $\hat{\mathbf{C}}_{XX} := \mathbf{C}_{XX} + \sigma_Y^2 \mathbf{K}_{ZZ}$

The purpose of the *Bayesian-consistency* kernel $\kappa_{bc} : \mathbb{X} \times \mathbb{X} \rightarrow \mathbb{R}$ is to relate the observation model in the state space to its counterpart in the RKHS. It models the correlations between the ‘components’ of $\varphi(\cdot)$ such that consistency is maintained with the flow map, i.e., ensuring that that $\mathbf{F}(\cdot)$ is an observable of the Koopman operator. The random variable $\nu_i \in \mathbb{H}$ is defined by the covariance operator $\mathcal{C}_{bc} : \mathbb{H} \rightarrow \mathbb{H}$, which in practice is required to be self-adjoint and invertible, and represents the statistical properties of the noisy full-state observable within the RKHS. For more details refer to Appendix E.

Similar to scalar-valued GP regression, our prior beliefs about the statistical properties of the operator $\mu_{Y|\cdot} : \mathbb{X} \rightarrow \mathbb{H}$ are represented by a GP, $\mu_{Y|\cdot} \sim \mathcal{GP}^\infty(\mathcal{M}_{pr}, \xi_{pr})$ ¹. However, here we are defining the prior covariance $\xi_{pr} : \mathbb{X} \times \mathbb{X} \rightarrow \mathbb{H} \otimes \mathbb{H}$ with an *operator-valued* kernel [Kadri et al., 2016]. Then, without loss of generality, we choose the mean operator $\mathcal{M}_{pr} : \mathbb{X} \rightarrow \mathbb{H}$ such that it produces an identically zero function. It follows that the prior distribution over the latent operator evaluations $\mu_{Y|\mathbf{X}} := \mathcal{P}_\varepsilon \Phi_X \in \mathbb{H}^{1 \times N}$ is

$$p_{pr}(\mu_{Y|\mathbf{X}}) = \mathcal{GP}^N(\mu_{Y|\mathbf{X}}; \mathcal{M}_{pr}(\mathbf{X}), \Xi_{XX}),$$

where Ξ_{XX} is the prior covariance evaluated at (\mathbf{X}, \mathbf{X}) and hence an element of $(\mathbb{H} \otimes \mathbb{H})^{N \times N}$.

The *Riesz–Fréchet representation theorem* [Hsing and Eubank, 2015, Fréchet, 1904] says that for each $\mathbf{x} \in \mathbb{X}$ and $g \in \mathbb{H}$, there is an element $\Xi(\mathbf{x})g : \mathbb{X} \rightarrow \mathbb{H}$, such that the reproducing property is

$$\langle \mu_{Y|\cdot}, \Xi(\mathbf{x})g \rangle_{\mathbb{H}^\mathbb{X}} = \langle \mu_{Y|\mathbf{x}}, g \rangle_{\mathbb{H}}.$$

This implies that the feature map $\Xi(\mathbf{x})$ is a bounded linear operator, $\Xi(\mathbf{x}) \in \mathfrak{B}(\mathbb{H}, \mathbb{H}^\mathbb{X})$, where $\mathbb{H}^\mathbb{X}$ denotes the \mathbb{H} -valued RKHS on \mathbb{X} (i.e., $\mu_{Y|\cdot} \in \mathbb{H}^\mathbb{X}$). Thereby, the relationship between the reproducing kernel $\xi_{pr}(\cdot, \cdot)$ and its associated feature map $\Xi(\mathbf{x})$ is

$$\langle \Xi(\mathbf{x})g, \Xi(\mathbf{x}')g' \rangle_{\mathbb{H}^\mathbb{X}} = \langle g, \xi_{pr}(\mathbf{x}, \mathbf{x}')g' \rangle_{\mathbb{H}}.$$

The entry at $(\xi_{pr}(\mathbf{x}, \mathbf{x}'))_{\mathbf{y}, \mathbf{y}'}$ determines the prior covariance between $\mu_{Y|\mathbf{x}}(\mathbf{y})$ and $\mu_{Y|\mathbf{x}'}(\mathbf{y}')$, i.e., it expresses the degree to which the response at (\mathbf{x}, \mathbf{y}) is affected by $(\mathbf{x}', \mathbf{y}')$ — before incorporating data.

Definition 2.1 models the lifted targets as scalar-valued GPs, and therefore the likelihood can be expressed as $p(\varphi(\mathbf{y}) | \mathcal{P}_\varepsilon, \mathbf{x}) = \mathcal{GP}(\mu_{Y|\mathbf{x}}, \sigma_Y^2 \kappa_{bc})$. Thereby, the posterior retains the same structure as in the scalar-valued case [Alvarez et al., 2012, Micchelli and Pontil, 2004, 2005]:

$$\mathcal{M}_{pst}(\mathbf{x}) := \mathcal{A} \xi_X(\mathbf{x}) = \sum_{i=1}^N \mathcal{A}_i \xi_{pr}(\mathbf{x}_i, \mathbf{x}), \quad (2.1)$$

$$\xi_{pst}(\mathbf{x}, \mathbf{x}') := \xi_{pr}(\mathbf{x}, \mathbf{x}') - \xi_X^\top(\mathbf{x}) \tilde{\Xi}_{XX}^{-1} \xi_X(\mathbf{x}'). \quad (2.2)$$

We unpack these equations by concatenating the noisy targets ‘end-to-end’ in $\Upsilon^\top := \text{vec}(\Phi_Y) \in \mathbb{H}^{\oplus N}$. We denote the weight operator by $\mathcal{A} := \Upsilon \tilde{\Xi}_{XX}^{-1}$, the noisy covariance operator by $\tilde{\Xi}_{XX} := \Xi_{XX} + \Sigma$, and the feature “vector” by $\xi_X(\mathbf{x}) := [\xi_{pr}(\mathbf{x}_1, \mathbf{x}), \dots, \xi_{pr}(\mathbf{x}_N, \mathbf{x})]^\top$.

We will elaborate on this point in Section 2.4, but the structure the operator-valued kernel is restricted to $\xi_{pr}(\mathbf{x}, \mathbf{x}') = \kappa_{pr}(\mathbf{x}, \mathbf{x}') \mathcal{C}_{bc}$. This form allows us to express the covariance operators in terms of the prior covariances over latent values of the flow map and Kronecker tensor products with \mathcal{C}_{bc} , i.e., $\Xi_{XX} := \mathbf{K}_{XX} \otimes \mathcal{C}_{bc}$ where $\mathbf{K}_{XX} := \Phi_X^\top \Phi_X \in \mathbb{R}^{N \times N}$. Similarly, the “sensor” noise covariance operator is denoted by $\Sigma := \mathbf{I}_N \otimes \sigma_Y^2 \mathcal{C}_{bc}$, and the feature vector is $\xi_X(\mathbf{x}) = \mathbf{k}_X(\mathbf{x}) \otimes \mathcal{C}_{bc}$ where $\mathbf{k}_X(\mathbf{x}) := \Phi_X^\top \varphi(\mathbf{x})$. Thereby, in essence we are implementing an *intrinsic model of coregionalization* [Alvarez et al., 2012].

Then by recalling the mixed matrix-vector product property: $(\mathbf{A} \otimes \mathbf{B}) \text{vec}(\mathbf{C}) = \text{vec}(\mathbf{BCA}^\top)$, the posterior mean (2.1) of the embedded PFO reduces to

$$\begin{aligned} \mathcal{M}_{pst}(\mathbf{x}) &= (\mathbf{k}_X^\top(\mathbf{x}) \otimes \mathcal{C}_{bc}) (\mathbf{K}_{XX} \otimes \mathcal{C}_{bc} + \mathbf{I}_N \otimes \sigma_Y^2 \mathcal{C}_{bc})^{-1} \Upsilon^\top \\ &= (\mathbf{k}_X^\top(\mathbf{x}) \tilde{\mathbf{K}}_{XX}^{-1} \otimes \mathcal{I}) \text{vec}(\Phi_Y) \\ &= \Phi_Y \tilde{\mathbf{K}}_{XX}^{-1} \Phi_X^\top \varphi(\mathbf{x}) = \mathbb{E}[\mathcal{P}_\varepsilon \varphi(X) | X = \mathbf{x}]. \end{aligned} \quad (2.3)$$

Hence, we recover the same expression for \mathcal{P}_ε derived in [Klus et al., 2020b], while also mirroring the frequentist approach of [Grünewälder et al., 2012]. In the expression of the mean, the operator \mathcal{C}_{bc} plays no role whatsoever, yet we observe that the posterior covariance over $\mathcal{P}_\varepsilon \varphi(\mathbf{x})$ retains the same form as the prior: $\xi_{pst}(\mathbf{x}, \mathbf{x}') = \kappa_{pst}(\mathbf{x}, \mathbf{x}') \mathcal{C}_{bc}$, i.e., a linear transformation of the covariance over the flow map.

¹The superscript attached to \mathcal{GP} indicates the dimensionality of the random object associated with the Gaussian process.

In the case where $D > 1$, we may want to treat the prior and Bayesian-consistency kernels as matrix-valued and include *anisotropic* measurement noise [Alvarez et al., 2012, Wilson et al., 2012]. However, for the rest of this manuscript we will continue assuming that the channels in the flow map are unrelated and that the sensor noise is isotropic.

2.2 Sparse Variational Bayesian Transfer Operators

Compressing the exact posterior to a smaller basis dictionary $\Phi_Z := \{\varphi(\mathbf{z}_i)\}_{i=1}^M \in \mathbb{H}^{1 \times M}$ with $M < N$, is possibly the easiest step, and demonstrates how straightforward it is to apply Gaussian process techniques to kernel transfer operators. Because, once we have framed the problem within a Bayesian framework, we can simply apply the variational free energy (VFE) method (see Appendix A.3 and Titsias [2009]):

$$\begin{aligned} \mathcal{M}_{\text{pst}}(\mathbf{x}) &= \xi_Z^\top(\mathbf{x}) (\Xi_{ZX} \Xi_{ZX}^\top + \Sigma \Xi_{ZZ})^{-1} \Xi_{ZX} \Upsilon^\top \\ &= (\mathbf{k}_Z^\top(\mathbf{x}) \tilde{\mathbf{C}}_{XX}^{-1} \otimes \mathcal{I}) \text{vec}(\Phi_Y \mathbf{K}_{ZX}^\top) \\ &= \Phi_Y \mathbf{K}_{ZX}^\top \tilde{\mathbf{C}}_{XX}^{-1} \Phi_Z^\top \varphi(\mathbf{x}), \end{aligned} \quad (2.4)$$

where we have the compressed covariance operators $\Xi_{ZX} := \mathbf{K}_{ZX} \otimes \mathcal{C}_{\text{bc}}$ and $\Xi_{ZZ} := \mathbf{K}_{ZZ} \otimes \mathcal{C}_{\text{bc}}$. The sparse covariance matrices $\mathbf{K}_{ZX} := \Phi_Z^\top \Phi_X$, $\mathbf{K}_{ZZ} := \Phi_Z^\top \Phi_Z$ allow us to define the noisy Gramian $\tilde{\mathbf{C}}_{XX} := \mathbf{K}_{ZX} \mathbf{K}_{ZX}^\top + \sigma_Y^2 \mathbf{K}_{ZZ}$. Lastly the feature vectors are $\mathbf{k}_Z(\mathbf{x}) := \Phi_Z^\top \varphi(\mathbf{x})$ and $\xi_Z(\mathbf{x}) := \mathbf{k}_Z(\mathbf{x}) \otimes \mathcal{C}_{\text{bc}}$.

In addition to providing a means of learning a sparse dictionary, the VFE method offers convergence-rate guarantees [Burt et al., 2019] and can also be used for hyperparameter optimization. Hyperparameter tuning is another obstacle for kernel-based Koopman methods, since one should ideally design the reproducing kernel function such that the Koopman operator is represented in an RKHS that is both densely defined and closable [Ikeda et al., 2022]. Consequently, finding such a kernel function tends to be a delicate and time-consuming task.

2.3 Koopman Mode Decomposition

To obtain an explicit, numerically tractable expression for the kernel Koopman matrix we first assume that any observable function $g \in \mathbb{H}$ can be approximated with a negligible error (i.e., \mathbb{H} is an invariant subspace of the Koopman operator). We then proceed by taking the adjoint of the embedded PFO in (2.4) to find the posterior expression for the kernel Koopman operator. Discretizing this operator yields the *Koopman matrix* (see (B.3) in Appendix B.3):

$$\mathbf{U} = \tilde{\mathbf{C}}_{XX}^{-1} \mathbf{C}_{XY} \in \mathbb{R}^{M \times M}. \quad (2.5)$$

Notice that since $\mathbf{C}_{XY} := \mathbf{K}_{ZX} \mathbf{K}_{ZY}^\top$ and $\mathbf{K}_{ZY} := \Phi_Z^\top \Phi_Y$, equation (2.5) recovers the standard algorithm for EDMD [Klus et al., 2016]. In other words, the Bayesian approach we have followed produces the same expression as the least-squares approach of EDMD with a Tikhonov parameter, σ_Y^2 . Of course, since EDMD is valid for more general choices of dictionaries, the previous statement is only true for a kernel-based dictionary [Williams et al., 2015a].

Provided that the eigenvalues are non-degenerate and unique, the eigenvalue decomposition of \mathbf{U} determines the coefficients of the spectral and spatial components:

$$\mathbf{U} = \mathbf{W} \mathbf{\Lambda} \mathbf{V}_\kappa, \quad (2.6)$$

where $\mathbf{\Lambda} \in \mathbb{C}^{M \times M}$ is a diagonal matrix containing the discrete-time eigenvalues. The right eigenvectors $\mathbf{W} \in \mathbb{C}^{M \times M}$ contain the projection vectors onto the eigenfunction basis, whereas the left eigenvectors $\mathbf{V}_\kappa = \mathbf{W}^{-1}$ correspond to the modes of the observables $\mathbf{k}_Z(\cdot) = [\kappa_{\text{pr}}(\mathbf{z}_1, \cdot), \dots, \kappa_{\text{pr}}(\mathbf{z}_M, \cdot)]^\top$.

The *projected* modes with respect to the full-state observables, $\mathbf{V}_f \in \mathbb{C}^{M \times D}$, are found via

$$\mathbf{V}_f = \mathbf{\Lambda}^{-1} \mathbf{V}_\kappa \tilde{\mathbf{C}}_{XX}^{-1} \mathbf{K}_{ZX} \mathbf{Y}^\top. \quad (2.7)$$

The implication of (2.7) is that for a single-step prediction, the model in (2.10) is also the posterior mean of a GP prior placed on the flow map (using the dynamically evolved states \mathbf{Y} as the targets). The point is that we can perform DMD on a random variable associated with the Koopman operator while maintaining consistency with the nonlinear dynamics on the state manifold.

In Appendix D, we present the numerically stable and efficient algorithm (GP-TCCA) used in the experiments of Section 3 for computing equations (2.5)–(2.7).

2.4 Prediction Theory

To construct a procedure by which we can produce multi-step forecasts and quantify the model's confidence in those future estimates, we interpret the posterior covariance as *heteroskedastic* process noise (which naturally decreases as the size of the training set grows). Put differently, the Bayesian Koopman operator is a random variable which represents stochastic knowledge-dependent dynamics. Thereby, since the projected dynamical system is linear in \mathbb{R}^M , the time series $\{\mathbf{k}_Z(X_i)\}_{i=0}^k$ of random vectors can be described by a *stochastic difference equation* [Hansen and Sargent, 2013]:

$$\mathbf{k}_Z(X_k) = \mathbf{A}_\kappa^1 \mathbf{k}_Z(X_{k-1}) + \mathbf{L}_{\text{pst}}(X_{k-1})\boldsymbol{\omega}_k, \quad (2.8)$$

where $\boldsymbol{\omega}_k \sim \mathcal{N}^M(\mathbf{0}, \mathbf{I}_M)$ and the multi-step transition matrix is $\mathbf{A}_\kappa^k := (\mathbf{W} \boldsymbol{\Lambda}^k \mathbf{V}_\kappa)^\top$. The process $\{\boldsymbol{\omega}_i\}_{i=1}^k$ is an i.i.d. *martingale difference sequence* adapted to the sequence of information sets $\{J_i\}_{i=0}^k$. Each *information set* J_k represents all the information available to an agent at time-step k , and contains all measurable functions of $\{X_0, \boldsymbol{\omega}_1, \dots, \boldsymbol{\omega}_k\}$.

The lower triangular matrix $\mathbf{L}_{\text{pst}}(X_k)$ is determined by the *Cholesky* decomposition of $\boldsymbol{\Xi}_{\text{pst}}^1(X_k)$. This covariance matrix encodes the one-step-ahead forecasting error of $\mathbf{k}_Z(X_k)$ conditioned on J_{k-1} . Given the operator-valued kernel defined earlier, in the current setting this matrix is $\boldsymbol{\Xi}_{\text{pst}}^1(X_k) = \kappa_{\text{pst}}^1(X_k, X_k) \mathbf{K}_{\text{bc}}$. Now recall that the expression for the sparse posterior kernel (see (A.6) in Appendix A.3) is

$$\kappa_{\text{pst}}(\mathbf{x}, \mathbf{x}') = \kappa_{\text{pr}}(\mathbf{x}, \mathbf{x}') - \mathbf{k}_Z^\top(\mathbf{x}) \tilde{\mathbf{B}} \mathbf{k}_Z(\mathbf{x}') \quad (2.9)$$

where $\tilde{\mathbf{B}} := (\mathbf{K}_{ZZ}^{-1} - \sigma_Y^2 \tilde{\mathbf{C}}_{XX}^{-1})$. Hence, the single-step prediction error is represented by the discretized version of the posterior kernel $\xi_{\text{pst}}(\cdot, \cdot)$ and subsequently the operator \mathcal{C}_{bc} (see Appendix E for details).

Expanding (2.8) into a recursive expression that is a function of $\{X_{k-j-1}, \boldsymbol{\omega}_{k-j}\}_{j=0}^{k-1}$ results in

$$\mathbf{k}_Z(X_k) = \mathbf{A}_\kappa^k \mathbf{k}_Z(X_0) + \sum_{j=0}^{k-1} \mathbf{A}_\kappa^j \mathbf{L}_{\text{pst}}(X_{k-j-1})\boldsymbol{\omega}_{k-j}.$$

Therefore, the mean vector of X_k given the realization \mathbf{x}_0 is

$$\hat{\mathbf{x}}_k = \mathbb{E}[X_k | X_0 = \mathbf{x}_0] = \mathbf{A}_f^k \mathbf{k}_Z(\mathbf{x}_0), \quad (2.10)$$

where the weight matrix is $\mathbf{A}_f^k := (\mathbf{W} \boldsymbol{\Lambda}^k \mathbf{V}_f)^\top \in \mathbb{R}^{D \times M}$. In deriving (2.10) we used (2.7), the relationship $X_k = (\mathbf{W} \mathbf{V}_f)^\top \mathbf{k}_Z(X_k)$, and the fact that a linear transformation of a Gaussian random vector yields another Gaussian random vector [Peebles Jr, 2001]. This last property was the key to calculating the Bayesian-consistency matrix $\mathbf{K}_{\text{bc}} \in \mathbb{R}^{M \times M}$ and enforcing the structure of the operator-valued prior covariance function to $\xi_{\text{pr}}(\mathbf{x}, \mathbf{x}') = \kappa_{\text{pr}}(\mathbf{x}, \mathbf{x}') \mathcal{C}_{\text{bc}}$.

The consistency between the generative models of the lifted space and the state space, rests on the knowledge that the following expression has to hold when linearly projecting the posterior covariance of the Gaussian random vectors:

$$\mathbf{K}_{\text{pst}}^k(\mathbf{x}) + \sigma_Y^2 \mathbf{I}_D = \mathbf{A}_f^0 (\boldsymbol{\Xi}_{\text{pst}}^k(\mathbf{x}) + \sigma_Y^2 \mathbf{K}_{\text{bc}}) (\mathbf{A}_f^0)^\top. \quad (2.11)$$

Given the independence assumption we placed on the components of the flow map, the single-step covariance matrix with respect to the full-state observables is $\mathbf{K}_{\text{pst}}^1(\mathbf{x}) = \kappa_{\text{pst}}^1(\mathbf{x}, \mathbf{x}) \mathbf{I}_D$. Hence, it follows that discretizing the operator \mathcal{C}_{bc} leads to

$$\mathbf{K}_{\text{bc}} = \left((\mathbf{A}_f^0)^\top \mathbf{A}_f^0 \right)^\dagger = \mathbf{V}_\kappa^* (\mathbf{V}_f \mathbf{V}_f^*)^\dagger \mathbf{V}_\kappa.$$

Where the Hermitian adjoint is indicated by $*$, and since the matrix \mathbf{K}_{bc} always has a rank less than or equal to D , we employed the Moore–Penrose pseudoinverse \dagger .

Now we are in a position to delve into the theory that describes how to propagate the covariance matrix $\boldsymbol{\Xi}_{\text{pst}}^k(\mathbf{x}_0)$. Thus, we start with the expression for the k -step prediction error:

$$\zeta_k := \mathbf{k}_Z(X_k) - \mathbf{k}_Z(\hat{\mathbf{x}}_k) = \sum_{j=0}^{k-1} \mathbf{A}_\kappa^j \mathbf{L}_{\text{pst}}(X_{k-j-1})\boldsymbol{\omega}_{k-j},$$

which results in the propagated covariance matrix with respect to the observables $\mathbf{k}_Z(\cdot)$:

$$\begin{aligned}\Xi_{\text{pst}}^k(X_0) &= \mathbb{E} \left[\zeta_k \zeta_k^\top \mid J_k \right] \\ &= \mathbb{E} \left[\sum_{j=0}^{k-1} \mathbf{A}_\kappa^j \Xi_{\text{pst}}^1(X_{k-j-1}) (\mathbf{A}_\kappa^j)^\top \mid J_k \right].\end{aligned}$$

As this expression is in general not analytically tractable, similar to Girard *et al.* [2002a,b] we can approximate it by performing Monte Carlo sampling or, if efficiency is of greater concern than accuracy, a *second-order Taylor* series expansion about the predicted mean²:

$$\mathbb{E} \left[\Xi_{\text{pst}}^1(X_k) \mid \mathbf{x}_0 \right] \approx \Xi_{\text{pst}}^1(\hat{\mathbf{x}}_k) + \mathbf{H}^k(\mathbf{x}_0),$$

where we have defined the curvature correction term as

$$\mathbf{H}^k(\mathbf{x}_0) := \frac{1}{2} \text{Tr} \left(\nabla^2(\hat{\mathbf{x}}_k) \mathbf{K}_{\text{pst}}^k(\mathbf{x}_0) \right) \mathbf{K}_{\text{bc}},$$

and $\nabla^2(\mathbf{x})$ as the $D \times D$ *Hessian* matrix³ of $\kappa_{\text{pst}}(\mathbf{x}, \mathbf{x})$.

Putting it all together we can obtain a recursive expression for the k -step covariance matrix:

$$\Xi_{\text{pst}}^k(\mathbf{x}_0) \approx \Xi_{\text{pst}}^1(\hat{\mathbf{x}}_{k-1}) + \mathbf{H}^{k-1}(\mathbf{x}_0) + \mathbf{U}^\top \Xi_{\text{pst}}^{k-1}(\mathbf{x}_0) \mathbf{U}, \quad (2.12)$$

which we can interpret as iteratively accumulating the prediction errors arising from random ‘shocks’ at each intermediate step, and where the magnitude of these shocks are dependent on the system’s state.

If all the eigenvalues of \mathbf{U} have magnitudes less than 1, then the effect of the shocks will diminish as the errors are propagated (i.e. the process is covariance-stationary); for eigenvalues with magnitudes equal to 1 the effect of the shocks will persist within the process, and for eigenvalues with amplitudes greater than 1 the effects are amplified. However, we should be cognizant of the fact that the Koopman operator is a *positive Markov operator* [Mauroy *et al.*, 2020], and will always have one ‘trivial’ mode with a unity eigenvalue and a constant-one eigenfunction as a fixed point.

Additionally, it is straightforward to adapt (2.12) such that it is valid for arbitrary choices of observables. For example, the expression, $\mathbf{W}^* \Xi_{\text{pst}}^k(\mathbf{x}_0) \mathbf{W}$, is the k -step covariance matrix of the eigenfunctions. This ability to compute the prediction error for eigenfunctions are showcased in Figures 5 and 6, while the propagated errors are illustrated in Figure 1.

2.5 Model Selection

Hyperparameter optimization proceeds as if one were only interested in learning the optimal feature space for the flow map with the VFE method [Titsias, 2009]. This is an optimization problem that is solved by maximizing the sum of the VFEs of each of the components of the flow map $\mathbf{F} = \{f_i\}_{i=1}^D$. The reasoning is that the theoretical Bayesian-consistent structure of our model also ensures a coherent parameterization of the kernel Koopman and Perron–Frobenius operators.

It is important to recognize that optimizing the pseudo-inputs \mathbf{Z} even with analytic gradients can be computationally overwhelming. As a compromise, we recommend a layered greedy approach starting with the active learning methods of [MacKay, 1992, Engel *et al.*, 2004, Lawrence and Platt, 2004]. These methods are computationally very efficient, since they only require rank-one updates. While these approaches focus more on finding a good ‘spread’ of dictionary functions, the VFE method, in comparison, learns a dictionary that shapes the feature space to suit the observed targets.

Thereby, we used the approximate linear dependence (ALD) selection criterion [Engel *et al.*, 2004] as a first pass to determine a subset of candidate locations for the pseudo-inputs from the training inputs. Since the ALD approach is a local ‘whack-a-mole’ active learning scheme, we followed it up by implementing *active learning Cohn* [Seo *et al.*, 2000]: a more globally oriented methodology that approximates a full A-optimal design [Gramacy, 2020]. As a last step, only after a predefined number of new dictionary functions had been identified was the VFE hyperparameter tuning algorithm activated, with the greedy results given as a warm start⁴. This process is interleaved with the adaptation of generative hyperparameters, and repeats until no more pseudo-inputs are added to the basis dictionary or a threshold is passed, e.g., an upper limit on the dictionary size.

²The *unscented transform* is also an alternative and very attractive approach [Julier and Uhlmann, 2004].

³For stationary kernels the quadratic form of (2.9) enables an approximation of $\nabla^2(\mathbf{x})$ that requires only gradient information [Nocedal and Wright, 2006].

⁴One could consider including other *Subset of Data* algorithms, e.g. [Vincent and Bengio, 2002, Dhillon *et al.*, 2004].

3 Numerical Experiments

With the foundational unification of GP regression and DMD complete, we present the results obtained from a few experiments. In all of the experiments, we used the Matérn^{5/2} kernel [Matérn, 2013] with automatic relevance determination (ARD; Rasmussen and Williams [2006]):

$$\kappa(\mathbf{x}, \mathbf{x}') = \sigma_f^2 \left(1 + \sqrt{5} r + \frac{5}{3} r^2 \right) \exp(-\sqrt{5} r).$$

where $r^2 = (\mathbf{x} - \mathbf{x}')^\top \mathbf{T}^{-1}(\mathbf{x} - \mathbf{x}')$. The matrix $\mathbf{T} \succ 0$ is diagonal and contains generative hyperparameters referred to as the *characteristic lengthscales*. These variables effectively prioritize the different components of \mathbf{x} and \mathbf{x}' and quantify how far it is needed to move along a particular axis for the function values to become uncorrelated. The hyperparameter σ_f^2 , called the *signal variance*, represents the average distance squared of the regression function from its mean.

For all numerical experiments, the data was standardized, and we emphasize that the data collection setup was asymmetric with respect to measurement noise. Since our model is not theoretically equipped to account for sensor noise on the inputs, we restricted the corruption to the dynamically evolved states. This simplification is admissible in surrogate modeling, but unrealistic in the majority of physical data acquisition contexts.

3.1 Generalization Errors

We compared the multi-step errors of our algorithm (referred to as GP-TCCA) using the *Van der Pol oscillator* as a benchmark:

$$\begin{aligned} \dot{x}_{t,1} &= x_{t,2}, \\ \dot{x}_{t,2} &= \alpha(1 - x_{t,1}^2)x_{t,2} - x_{t,1}, \end{aligned}$$

where $\alpha = 2$ controls the degree of nonlinearity. The dynamical system was simulated by a numerical ODE solver and sampled in time intervals of $\Delta t = 50.0$ [ms]. Figure 1 depicts an example trajectory of the oscillator and its associated forecast.

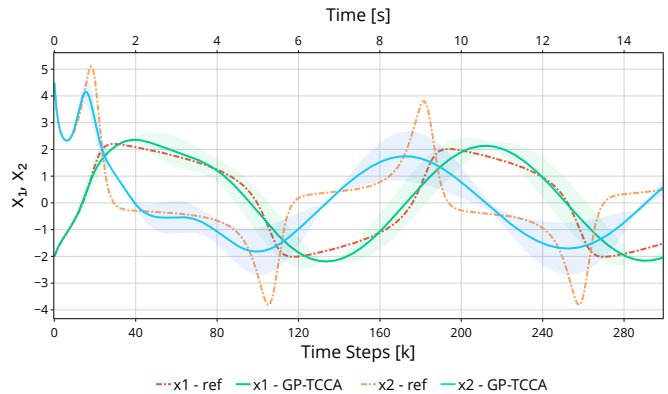


Figure 1: Multi-step predictions (solid lines) with 95.45% confidence intervals (shaded regions), and reference values (dashed lines), c.f. Figure 4.

The metric used to quantify the generalization errors over a test set of $N_{\text{tst}} = 5000$ noise-free samples was the symmetric mean absolute percentage error (SMAPE; Nguyen et al. [2019]):

$$SMAPE = 100\% \frac{3}{N_{\text{tst}}} \sum_{i=1}^{N_{\text{tst}}} \frac{\|\mathbf{y}_i - \hat{\mathbf{y}}_i\|}{\|\mathbf{y}_i\| + \|\hat{\mathbf{y}}_i\|}.$$

The SMAPE equals 100% if all the model predictions are twice the testing values, i.e., $\hat{\mathbf{y}}_i = 2\mathbf{y}_i$.

As depicted in Figure 2, alongside our model we implemented *two* more models and compared their accuracies over multi-step predictions. The first algorithm that we compared ours to is ‘Exact (Extended) DMD’ [Tu et al., 2014], and the second is a sparse GP model of the flow map [Titsias, 2009]. When comparing across the three algorithms, all three models shared the same set of hyperparameters.

We also compared the VFE method to the ‘variational approach to Markov processes’ (VAMP) for hyperparameter optimization [Wu and Noé, 2020]. Specifically we maximized the VAMP-2 score of the model.

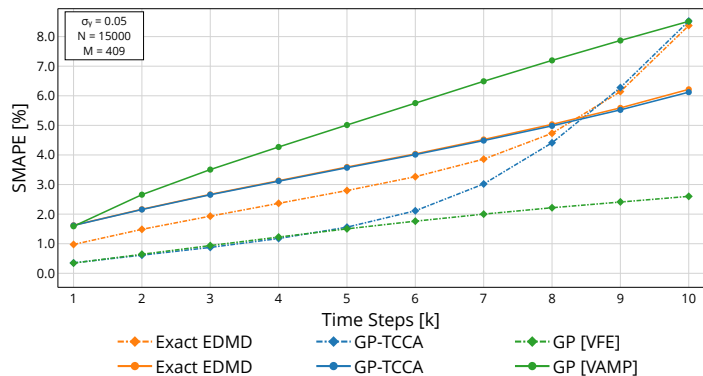


Figure 2: *Generalization errors*. Comparing SMAPE over multi-step forecasts of GP-TCCA (blue), Exact DMD (orange), and a variational sparse GP (green), with hyperparameters found via VFE (dashed) and VAMP-2 (solid), c.f. Figure 3.

When optimizing the VAMP score, the two DMD algorithms are virtually indistinguishable, suggesting that the Tikhonov regularization has little to no effect. This indicates that the VAMP-2 objective does not capture sensor noise as effectively as maximizing the VFE of the flow map. Figure 2 shows that our GP-DMD variant outperforms Exact EDMD under noisy conditions. This aligns with our expectations given the explicit treatment of sensor noise and the additional structure imposed by the Bayesian model. However, the nonlinear growth did prompt a closer examination of our regularization strategy.

3.2 Decoupling the Lifted Observation Model

To assess the sensitivity of our algorithm to the approximation introduced in Definition 2.1, we separately train a regularization parameter for the lifted model using the kernelized targets \mathbf{K}_{ZY} (after estimating the optimal kernel hyperparameters and pseudo-inputs as discussed in Section 2.5). In effect, we are defining the RKHS noise model with $\sigma_Y^2 \kappa_{bc}(\cdot, \cdot)$ where σ_Y^2 is not directly coupled to the variance of the sensor noise in the state space, σ_Y^2 . Put differently, the regularization parameter in (2.5) now corresponds to σ_Y , whereas in (2.7) it is still σ_Y . This establishes a division of roles between the two regularization terms: σ_Y is predominantly responsible for projecting to the state space, while σ_Y controls the accuracies of the multi-step forecasts. Consequently, the relationship in (2.11) does not hold exactly anymore, but our model is more flexible.

The effect of decoupling is illustrated in Figure 3 where we observe that the growth rate of the GP-TCCA model has markedly reduced, leading to more accurate long-term predictions. We therefore increase the credence in our hypothesis: rigorously accounting for the distortion introduced by the nonlinear feature map will yield a more robust model. For example, we are naturally tempted to model the statistical properties of ν_i as non-Gaussian and input-dependent (i.e., heteroskedastic). This is apparent when we notice that $\kappa_{pr}(\mathbf{x}, Y)$ is typically a nonlinear many-to-one transformation of Y .

3.3 Rejections

Although the GP model attains the lowest error, the DMD variants are more computationally efficient, because multi-step forecasts follow from spectral propagation (i.e., raising the eigenvalue matrix to the desired power). In contrast, a purely GP-based rollout must repeatedly lift each intermediate state, increasing computational overhead. Consequently, for long horizons, DMD methods often employ a reprojec-tion scheme that combines both approaches; intermittent rejections onto the state manifold mitigates drift arising from the fact that the learned finite-dimensional subspace may not be perfectly invariant under the true Koopman operator [Van Goor et al., 2023].

In Figure 4 we demonstrate how rejections based on a mechanism defined on (2.12) can be effectively used to decrease the computational cost while also maintaining accuracy. The idea was simply to reproject when the Euclidean norm of the diagonal entries in $\mathbf{K}_{pst}^k(\mathbf{x}_0)$ exceeded some predefined tolerance. At such points, the current estimate $\hat{\mathbf{x}}_k$ was treated as a noise-free measurement, and the feature vector $\mathbf{k}_Z(\hat{\mathbf{x}}_k)$ was recomputed⁵.

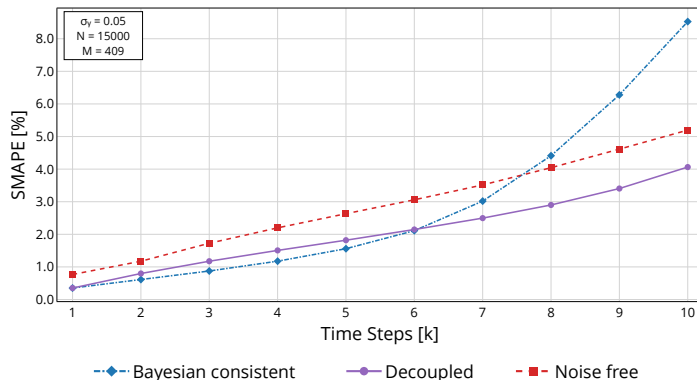


Figure 3: Generalization errors of the decoupled model. Blue: $\sigma_Y = \sigma_Y$, purple: $\sigma_Y \neq \sigma_Y$, red: $\sigma_Y = 0$, c.f. Figure 2.

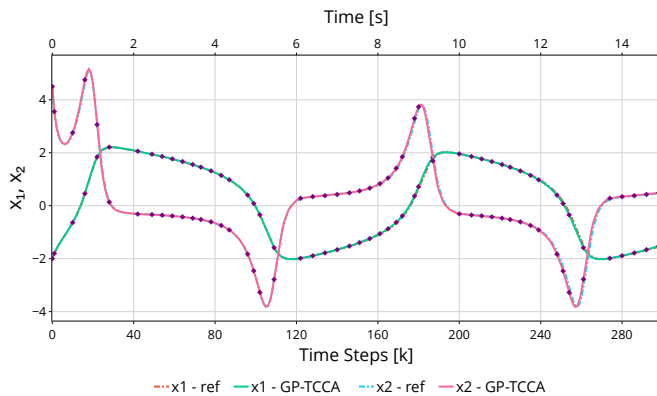


Figure 4: Multi-step predictions (solid lines) with rejections (diamond markers), c.f. Figure 1.

⁵In evaluating $\Xi_{pst}^1(\mathbf{x}) = \kappa_{pst}(\mathbf{x}, \mathbf{x}) \mathbf{K}_{bc}$ and subsequently (2.9), we employed spectral propagation with \mathbf{V}_κ to compute

For the depicted trajectory, on average a reprojection was performed after every 5 time-steps. In other words, the length of the forecasting horizons vary over the state space as the model automatically incorporates its epistemic uncertainty into the predictions. Interestingly, the regions where the vector field changes slowly is where the forecasting horizons are shorter, which suggest that errors accumulate faster in these regions.

3.4 Eigenfunction Uncertainty Quantification

The second dynamical system that we analyzed was the *stochastic well* problem described by the overdamped Langevin equation:

$$\begin{aligned} dx_{t,1} &= -\nabla_{x_1} V(\mathbf{x}_t) dt + \sigma_T dW_{t,1}, \\ dx_{t,2} &= -\nabla_{x_2} V(\mathbf{x}_t) dt + \sigma_T dW_{t,2}, \end{aligned}$$

where $W_{t,1}$ and $W_{t,2}$ are two independent standard Wiener processes. In our experiments, we fixed the noise intensity to $\sigma_T = 0.7$ and employed a sampling interval of $\Delta t = 10.0$ [s].

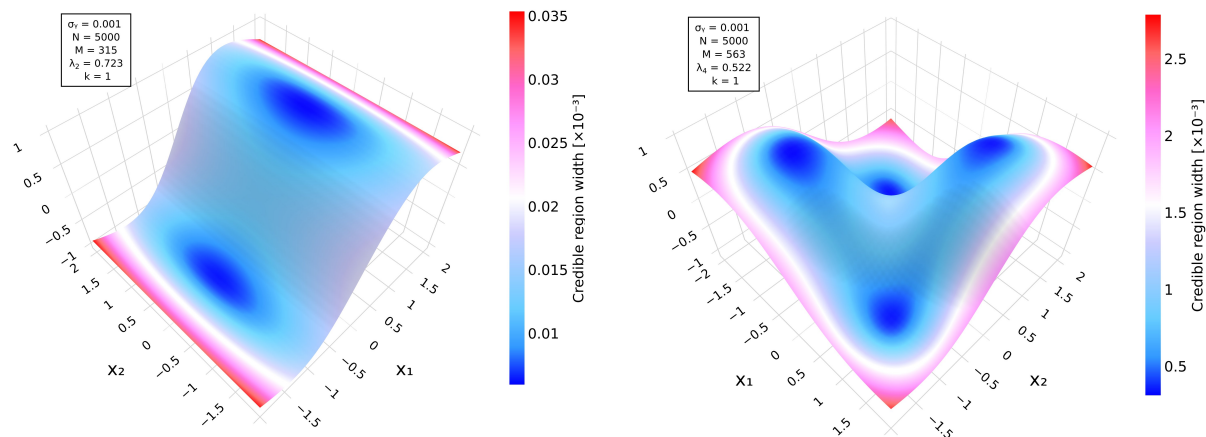


Figure 5: The 2nd eigenfunction of the stochastic double-well. The coloring illustrates the 68.27% confidence intervals.

When the potential function is $V(\mathbf{x}_t) = (x_{t,1}^2 - 1)^2 + x_{t,2}^2$, the system has two minima (or “wells”), separated by a barrier, representing the two metastable states of the system. Physically, a particle will spend long periods of time near one of the two minima and only rarely jump over the barrier to the other well due to random thermal fluctuations. By slightly altering the potential function we can increase the number of wells and dominant eigenfunctions. For example, the expression of the potential function for the quadruple-well system is $V(\mathbf{x}_t) = (x_{t,1}^2 - 1)^2 + (x_{t,2} - 1)^2$.

In the context of the double-well problem, the second eigenfunction, depicted in Figure 5, is the first and only non-trivial mode. This eigenfunction captures the switching between the two wells, and reveals the two-state structure and the slow timescale of the transitions [Klus et al., 2016]. In turn, the quadruple-well has three dominant non-trivial eigenfunctions, one of which we are depicting in Figure 6. Since these systems are reversible, the eigenvalues of the associated PFO and Koopman operators are exclusively real-valued [Mauroy et al., 2020].

Figures 5 and 6 show that the well locations align with regions of high certainty. This is because the dynamical systems spend most of their time around the wells, leading to dense sampling in these areas.

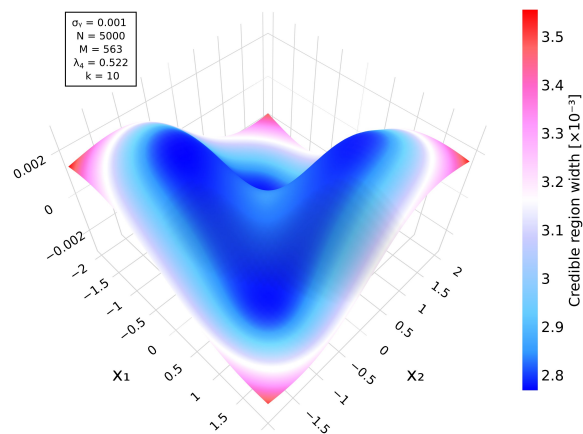


Figure 6: The 4th eigenfunction of the stochastic quadruple-well. The coloring depicts a one-standard deviation credible region.

the feature vector $\mathbf{k}_Z(\hat{\mathbf{x}}_k)$, thereby bypassing multiple evaluations of a potentially costly kernel function.

While the kernel lengthscales also influence the geometry of the low-uncertainty regions, the dominant effect in these plots is the sampling distribution of the training data sets: initial conditions were chosen based on an optimized Latin hypercube design [Bates et al., 2004, Urquhart et al., 2020], and succeeded by rolling out trajectories with lengths of 20 time-steps.

In the bottom plot of Figure 6, propagating the distribution over the eigenfunction forward in time reveals both a mixing and rescaling phenomenon: the eigenfunction collapses while the credible regions around the wells expand, ultimately spanning the entire sampling domain.

4 Conclusion

We have proposed a sparse kernel-based DMD algorithm which we formulated within a Bayesian framework that treats the embedded Perron–Frobenius operator [Klus et al., 2020b] as a random variable. By unifying operator learning with the mature field of Gaussian process regression the method extends EDMD by incorporating hyperparameter optimization, sparse dictionary learning, enables propagating uncertainties in the eigenfunctions of the flow map, and provides a criteria for reprojections.

The primary insight we have gained from the ablation studies is that kernel transfer operators could benefit from a non-Gaussian and a heteroskedastic observation model; one that is closely intertwined with a Bayesian consistent notion of an operator-valued RKHS. However, we have another reason to modify our model with a more complex noise model; thus far, we have only focused on compensating for measurement noise on the target variables. Yet, DMD is known to be susceptible to adverse effects arising from noise on the inputs [Dawson et al., 2016, Pan et al., 2021, Duke et al., 2012, Bagheri, 2014]. Incidentally, one approach to dealing with input-noise is a heteroskedastic GP model [Wilson et al., 2012, Lázaro-Gredilla and Titsias, 2011, McHutchon and Rasmussen, 2011]. Alternatively, in the Koopman community, several variants of DMD have been proposed to correct for the bias induced by input-noise [Hemati et al., 2017, Jiang and Liu, 2022, Scherl et al., 2020, Nonomura et al., 2019].

Earlier we posed the question of which philosophical stance is most appropriate for kernel transfer operators: a Bayesian or a frequentist perspective. We have argued that the Bayesian viewpoint offers ample opportunities to enrich the interpretation of DMD models. At the same time, we have also demonstrated that diverse perspectives can be especially valuable, as uncovering the reasons for discrepancies between the two paradigms led to the insights that solved the problem. Thus, rather than exclusively favoring one approach above the other, we advocate for employing Bayesian and frequentist methods in tandem whenever possible.

Funding

This work has been supported by the Ministry of Culture and Science of North Rhine-Westphalia (MKW NRW) within the project SAIL under the grant no. NW21-059D.

References

- Alexandre Mauroy, Y Susuki, and Igor Mezić. *The Koopman operator in systems and control*. Springer, 2020.
- Stefan Klus, Péter Koltai, and Christof Schütte. On the numerical approximation of the Perron–Frobenius and Koopman operator. *Journal of Computational Dynamics*, 3(1):51–79, 2016. doi: 10.3934/jcd.2016003.
- Steven L. Brunton, Marko Budišić, Eurika Kaiser, and J. Nathan Kutz. Modern Koopman theory for dynamical systems. *SIAM Review*, 64(2):229–340, 2022. doi: 10.1137/21M1401243. URL <https://doi.org/10.1137/21M1401243>.
- Carl Edward Rasmussen and Christopher K. I. Williams. *Gaussian Processes for Machine Learning*. Adaptive Computation and Machine Learning. MIT Press, Cambridge, MA, 2006. ISBN 9780262182539. URL <http://www.gaussianprocess.org/gpml/>.
- J Shawe-Taylor. Kernel methods for pattern analysis. *Cambridge University Press google schola*, 2: 181–201, 2004.
- Alain Berlines and Christine Thomas-Agnan. *Reproducing kernel Hilbert spaces in probability and statistics*. Springer Science & Business Media, 2011.
- Noel Cressie. The origins of Kriging. *Mathematical geology*, 22:239–252, 1990.
- Thomas Hofmann, Bernhard Schölkopf, and Alexander J. Smola. Kernel methods in machine learning. *The Annals of Statistics*, 36(3):1171 – 1220, 2008. doi: 10.1214/009053607000000677. URL <https://doi.org/10.1214/009053607000000677>.
- Bernhard Schölkopf and Alexander J Smola. *Learning with kernels: support vector machines, regularization, optimization, and beyond*. MIT press, 2002.
- Marko Budišić, Ryan Mohr, and Igor Mezić. Applied Koopmanism. *Chaos: An Interdisciplinary Journal of Nonlinear Science*, 22(4), 2012.
- Saburo Saitoh, Yoshihiro Sawano, et al. *Theory of reproducing kernels and applications*. Springer, 2016.
- Clarence W Rowley, Igor Mezić, Shervin Bagheri, Philipp Schlatter, and Dan S Henningson. Spectral analysis of nonlinear flows. *Journal of fluid mechanics*, 641:115–127, 2009.
- Yoshihiko Susuki and Igor Mezić. Nonlinear Koopman modes and coherency identification of coupled swing dynamics. *IEEE Transactions on Power Systems*, 26(4):1894–1904, 2011.
- Yoshihiko Susuki, Igor Mezić, and Takashi Hikiyama. Coherent swing instability of power grids. *Journal of nonlinear science*, 21:403–439, 2011.
- Erik Berger, Mark Sastuba, David Vogt, Bernhard Jung, and Heni Ben Amor. Estimation of perturbations in robotic behavior using dynamic mode decomposition. *Advanced Robotics*, 29(5):331–343, 2015.
- Daniel Bruder, Brent Gillespie, C. David Remy, and Ram Vasudevan. Modeling and control of soft robots using the Koopman operator and model predictive control. In *Proceedings of Robotics: Science and Systems (RSS)*, Freiburg im Breisgau, Germany, June 2019. doi: 10.15607/RSS.2019.XV.060.
- Marcos Netto and Lamine Mili. A robust data-driven Koopman Kalman filter for power systems dynamic state estimation. *IEEE Transactions on Power Systems*, 33(6):7228–7237, 2018.
- Igor Mezić. Spectrum of the Koopman operator, spectral expansions in functional spaces, and state space geometry, 2019. URL <https://arxiv.org/abs/1702.07597>.
- Bernard O Koopman. Hamiltonian systems and transformation in Hilbert space. *Proceedings of the National Academy of Sciences*, 17(5):315–318, 1931.
- Bernard O Koopman and J v Neumann. Dynamical systems of continuous spectra. *Proceedings of the National Academy of Sciences*, 18(3):255–263, 1932.

- Qianxiao Li, Felix Dietrich, Erik M Bollt, and Ioannis G Kevrekidis. Extended dynamic mode decomposition with dictionary learning: A data-driven adaptive spectral decomposition of the Koopman operator. *Chaos: An Interdisciplinary Journal of Nonlinear Science*, 27(10), 2017.
- Naoya Takeishi, Yoshinobu Kawahara, and Takehisa Yairi. Learning Koopman invariant subspaces for dynamic mode decomposition. *Advances in neural information processing systems*, 30, 2017.
- Christoph Wehmeyer and Frank Noé. Time-lagged autoencoders: Deep learning of slow collective variables for molecular kinetics. *The Journal of chemical physics*, 148(24), 2018.
- Enoch Yeung, Soumya Kundu, and Nathan Hodas. Learning deep neural network representations for Koopman operators of nonlinear dynamical systems. In *2019 American Control Conference (ACC)*, pages 4832–4839. IEEE, 2019.
- Omri Azencot, N Benjamin Erichson, Vanessa Lin, and Michael Mahoney. Forecasting sequential data using consistent Koopman autoencoders. In *International Conference on Machine Learning*, pages 475–485. PMLR, 2020.
- Hamidreza Eivazi, Luca Guastoni, Philipp Schlatter, Hossein Azizpour, and Ricardo Vinuesa. Recurrent neural networks and Koopman-based frameworks for temporal predictions in a low-order model of turbulence. *International Journal of Heat and Fluid Flow*, 90:108816, 2021.
- Andreas Mardt, Luca Pasquali, Hao Wu, and Frank Noé. Vampnets for deep learning of molecular kinetics. *Nature communications*, 9(1):5, 2018.
- Peter J Schmid. Dynamic mode decomposition of numerical and experimental data. *Journal of fluid mechanics*, 656:5–28, 2010.
- Matthew O Williams, Ioannis G Kevrekidis, and Clarence W Rowley. A data-driven approximation of the Koopman operator: Extending dynamic mode decomposition. *Journal of Nonlinear Science*, 25:1307–1346, 2015a.
- Matthew J Colbrook. The multiverse of dynamic mode decomposition algorithms. *Numerical Analysis meets Machine Learning*, 25:127, 2024.
- Matthew J Colbrook and Alex Townsend. Rigorous data-driven computation of spectral properties of Koopman operators for dynamical systems. *Communications on Pure and Applied Mathematics*, 77(1):221–283, 2024.
- Matthew O Williams, Clarence W Rowley, and Ioannis G Kevrekidis. A kernel-based method for data-driven Koopman spectral analysis. *Journal of Computational Dynamics*, 2(2):247–265, 2015b.
- Stefan Klus, Feliks Nüske, Sebastian Peitz, Jan-Hendrik Niemann, Cecilia Clementi, and Christof Schütte. Data-driven approximation of the Koopman generator: Model reduction, system identification, and control. *Physica D: Nonlinear Phenomena*, 406:132416, 2020a.
- Mathias Wanner and Igor Mezic. Robust approximation of the stochastic Koopman operator. *SIAM Journal on Applied Dynamical Systems*, 21(3):1930–1951, 2022.
- Nelida Črnjarić-Žic, Senka Maćešić, and Igor Mezić. Koopman operator spectrum for random dynamical systems. *Journal of Nonlinear Science*, 30:2007–2056, 2020.
- Matthew J Colbrook, Qin Li, Ryan V Raut, and Alex Townsend. Beyond expectations: residual dynamic mode decomposition and variance for stochastic dynamical systems. *Nonlinear Dynamics*, 112(3):2037–2061, 2024.
- Sebastian Peitz and Stefan Klus. Koopman operator-based model reduction for switched-system control of PDEs. *Automatica*, 106:184–191, 2019.
- Sebastian Peitz, Samuel E Otto, and Clarence W Rowley. Data-driven model predictive control using interpolated Koopman generators. *SIAM Journal on Applied Dynamical Systems*, 19(3):2162–2193, 2020.

- Joshua L Proctor, Steven L Brunton, and J Nathan Kutz. Dynamic mode decomposition with control. *SIAM Journal on Applied Dynamical Systems*, 15(1):142–161, 2016.
- Samuel E Otto and Clarence W Rowley. Koopman operators for estimation and control of dynamical systems. *Annual Review of Control, Robotics, and Autonomous Systems*, 4(1):59–87, 2021.
- Stefan Klus, Andreas Bitttracher, Ingmar Schuster, and Christof Schütte. A kernel-based approach to molecular conformation analysis. *The Journal of Chemical Physics*, 149(24), 2018.
- Anthony M DeGennaro and Nathan M Urban. Scalable extended dynamic mode decomposition using random kernel approximation. *SIAM Journal on Scientific Computing*, 41(3):A1482–A1499, 2019.
- Keisuke Fujii and Yoshinobu Kawahara. Dynamic mode decomposition in vector-valued reproducing kernel Hilbert spaces for extracting dynamical structure among observables. *Neural Networks*, 117: 94–103, 2019.
- Suddhasattwa Das and Dimitrios Giannakis. Koopman spectra in reproducing kernel Hilbert spaces. *Applied and Computational Harmonic Analysis*, 49(2):573–607, 2020.
- Suddhasattwa Das, Dimitrios Giannakis, and Joanna Slawinska. Reproducing kernel Hilbert space compactification of unitary evolution groups. *Applied and Computational Harmonic Analysis*, 54:75–136, 2021.
- Masahiro Ikeda, Isao Ishikawa, and Corbinian Schlosser. Koopman and Perron–Frobenius operators on reproducing kernel Banach spaces. *Chaos: An Interdisciplinary Journal of Nonlinear Science*, 32(12), 2022.
- Petar Bevanda, Max Beier, Armin Lederer, Stefan Sosnowski, Eyke Hüllermeier, and Sandra Hirche. Koopman kernel regression. *Advances in Neural Information Processing Systems*, 36, 2024.
- Stefan Klus, Ingmar Schuster, and Krikamol Muandet. Eigendecompositions of transfer operators in reproducing kernel Hilbert spaces. *Journal of Nonlinear Science*, 30:283–315, 2020b.
- Peter J Baddoo, Benjamin Herrmann, Beverley J McKeon, and Steven L Brunton. Kernel learning for robust dynamic mode decomposition: linear and nonlinear disambiguation optimization. *Proceedings of the Royal Society A*, 478(2260):20210830, 2022.
- Petar Bevanda, Max Beier, Armin Lederer, Alexandre Capone, Stefan Sosnowski, and Sandra Hirche. Koopman-equivariant Gaussian processes. *arXiv preprint arXiv:2502.06645*, 2025.
- Stefan Klus, Feliks Nüske, and Boumediene Hamzi. Kernel-based approximation of the Koopman generator and Schrödinger operator. *Entropy*, 22(7):722, 2020c.
- Friedrich M. Philipp, Manuel Schaller, Karl Worthmann, Sebastian Peitz, and Feliks Nüske. Error bounds for kernel-based approximations of the Koopman operator. *Applied and Computational Harmonic Analysis*, 71:101657, 2024. ISSN 1063-5203. doi: <https://doi.org/10.1016/j.acha.2024.101657>. URL <https://www.sciencedirect.com/science/article/pii/S1063520324000344>.
- David JC MacKay et al. Introduction to Gaussian processes. *NATO ASI series F computer and systems sciences*, 168:133–166, 1998.
- Agathe Girard, Carl Rasmussen, Joaquin Quiñero Candela, and Roderick Murray-Smith. Gaussian process priors with uncertain inputs application to multiple-step ahead time series forecasting. In S. Becker, S. Thrun, and K. Obermayer, editors, *Advances in Neural Information Processing Systems*, volume 15. MIT Press, 2002a.
- Jack Wang, Aaron Hertzmann, and David J Fleet. Gaussian process dynamical models. *Advances in neural information processing systems*, 18, 2005.
- Ercan Solak, Roderick Murray-Smith, WE Leithead, Douglas Leith, and Carl Rasmussen. Derivative observations in Gaussian process models of dynamic systems. *Advances in neural information processing systems*, 15, 2002.

- Michalis Titsias. Variational learning of inducing variables in sparse Gaussian processes. In *Artificial intelligence and statistics*, pages 567–574. PMLR, 2009.
- Matthew J Colbrook, Bogdan Roman, and Anders C Hansen. How to compute spectra with error control. *Physical Review Letters*, 122(25):250201, 2019.
- Matthew J Colbrook and Alex Townsend. Avoiding discretization issues for nonlinear eigenvalue problems. *SIAM Journal on Matrix Analysis and Applications*, 46(1):648–675, 2025.
- Matthew J Colbrook, Lorna J Ayton, and Máté Szőke. Residual dynamic mode decomposition: robust and verified Koopmanism. *Journal of Fluid Mechanics*, 955:A21, 2023.
- Trevor Hastie. The elements of statistical learning: data mining, inference, and prediction, 2009.
- Tomaso Poggio and Federico Girosi. Networks for approximation and learning. *Proceedings of the IEEE*, 78(9):1481–1497, 1990.
- Grace Wahba. *Spline models for observational data*. SIAM, 1990.
- Mohammad Tabish, Neil K Chada, and Stefan Klus. Learning dynamical systems from data: Gradient-based dictionary optimization. *Physica D: Nonlinear Phenomena*, page 134822, 2025.
- Hachem Kadri, Emmanuel Dufflos, Philippe Preux, Stéphane Canu, Alain Rakotomamonjy, and Julien Audiffren. Operator-valued kernels for learning from functional response data. *Journal of Machine Learning Research*, 17(20):1–54, 2016. URL <http://jmlr.org/papers/v17/11-315.html>.
- Tailen Hsing and Randall Eubank. *Theoretical foundations of functional data analysis, with an introduction to linear operators*, volume 997. John Wiley & Sons, 2015.
- Maurice Fréchet. Sur les opérations linéaires. *Transactions of the American Mathematical Society*, 5(4):493–499, 1904.
- Mauricio A Alvarez, Lorenzo Rosasco, Neil D Lawrence, et al. Kernels for vector-valued functions: A review. *Foundations and Trends in Machine Learning*, 4(3):195–266, 2012.
- Charles Micchelli and Massimiliano Pontil. Kernels for multi-task learning. *Advances in neural information processing systems*, 17, 2004.
- Charles A Micchelli and Massimiliano Pontil. On learning vector-valued functions. *Neural computation*, 17(1):177–204, 2005.
- Steffen Grünewälder, Guy Lever, Luca Baldassarre, Sam Patterson, Arthur Gretton, and M Pontil. Conditional mean embeddings as regressors. In *29th International Conference on Machine Learning (ICML 2012)*, pages 1823–1830. Omnipress, 2012.
- Andrew Gordon Wilson, David A. Knowles, and Zoubin Ghahramani. Gaussian process regression networks. In *Proceedings of the 29th International Conference on Machine Learning (ICML’12)*, page 1139–1146, Madison, WI, USA, 2012. Omnipress. ISBN 9781450312851.
- David Burt, Carl Edward Rasmussen, and Mark Van Der Wilk. Rates of convergence for sparse variational gaussian process regression. In *International Conference on Machine Learning*, pages 862–871. PMLR, 2019.
- Lars Peter Hansen and Thomas J. Sargent. *Chapter 2 Stochastic Linear Difference Equations*. Princeton University Press, 2013. ISBN 9780691042770.
- Peyton Z Peebles Jr. *Probability, random variables, and random signal principles*. McGraw-Hill, 2001.
- Agathe Girard, Carl Edward Rasmussen, and Roderick Murray-Smith. Gaussian process priors with uncertain inputs: Multiple-step ahead prediction. Technical Report TR-2002-119, Department of Computing Science, University of Glasgow, 2002b. URL <https://www.dcs.gla.ac.uk/~rod/publications/GirRasMur02-TR-2002-119.pdf>.

- S.J. Julier and J.K. Uhlmann. Unscented filtering and nonlinear estimation. *Proceedings of the IEEE*, 92(3):401–422, 2004. doi: 10.1109/JPROC.2003.823141.
- Jorge Nocedal and Stephen J. Wright. *Numerical Optimization*. Springer, 2 edition, 2006.
- David JC MacKay. Information-based objective functions for active data selection. *Neural computation*, 4(4):590–604, 1992.
- Yaakov Engel, Shie Mannor, and Ron Meir. The kernel recursive least-squares algorithm. *IEEE Transactions on signal processing*, 52(8):2275–2285, 2004.
- Neil D Lawrence and John C Platt. Learning to learn with the informative vector machine. In *Proceedings of the twenty-first international conference on Machine learning*, page 65, 2004.
- Sambu Seo, M. Wallat, T. Graepel, and K. Obermayer. Gaussian process regression: active data selection and test point rejection. In *Proceedings of the IEEE-INNS-ENNS International Joint Conference on Neural Networks. IJCNN 2000. Neural Computing: New Challenges and Perspectives for the New Millennium*, volume 3, pages 241–246 vol.3, 2000. doi: 10.1109/IJCNN.2000.861310.
- Robert B Gramacy. *Surrogates: Gaussian process modeling, design, and optimization for the applied sciences*. Chapman and Hall/CRC, 2020.
- Pascal Vincent and Yoshua Bengio. Kernel matching pursuit. *Machine learning*, 48(1):165–187, 2002.
- Inderjit S. Dhillon, Yuqiang Guan, and Brian Kulis. Kernel k-means: spectral clustering and normalized cuts. In *Proceedings of the Tenth ACM SIGKDD International Conference on Knowledge Discovery and Data Mining, KDD '04*, page 551–556, New York, NY, USA, 2004. Association for Computing Machinery. ISBN 1581138881. doi: 10.1145/1014052.1014118. URL <https://doi.org/10.1145/1014052.1014118>.
- Bertil Matérn. *Spatial variation*, volume 36. Springer Science & Business Media, 2013.
- Thieu Nguyen, Tu Nguyen, Binh Minh Nguyen, and Giang Nguyen. Efficient time-series forecasting using neural network and opposition-based coral reefs optimization. *International Journal of Computational Intelligence Systems*, 12(2):1144–1161, 2019.
- Jonathan H. Tu, Clarence W. Rowley, Dirk M. Luchtenburg, Steven L. Brunton, and J. Nathan Kutz. On dynamic mode decomposition: Theory and applications. *Journal of Computational Dynamics*, 2014. ISSN 2158-2491. doi: 10.3934/jcd.2014.1.391. URL <https://www.aimsocieties.org/article/id/1dfebc20-876d-4da7-8034-7cd3c7ae1161>.
- Hao Wu and Frank Noé. Variational approach for learning Markov processes from time series data. *Journal of Nonlinear Science*, 30(1):23–66, 2020.
- Pieter Van Goor, Robert Mahony, Manuel Schaller, and Karl Worthmann. Reprojection methods for Koopman-based modelling and prediction. In *2023 62nd IEEE Conference on Decision and Control (CDC)*, pages 315–321. IEEE, 2023.
- Stuart Bates, Johann Sienz, and Vassili Toropov. Formulation of the optimal latin hypercube design of experiments using a permutation genetic algorithm. In *45th aiaa/asme/asce/ahs/asc structures, structural dynamics & materials conference*, page 2011, 2004.
- Magnus Urquhart, Emil Ljungskog, and Simone Sebben. Surrogate-based optimisation using adaptively scaled radial basis functions. *Applied Soft Computing*, 88:106050, 2020.
- Scott TM Dawson, Maziar S Hemati, Matthew O Williams, and Clarence W Rowley. Characterizing and correcting for the effect of sensor noise in the dynamic mode decomposition. *Experiments in Fluids*, 57:1–19, 2016.
- Shaowu Pan, Nicholas Arnold-Medabalimi, and Karthik Duraisamy. Sparsity-promoting algorithms for the discovery of informative Koopman-invariant subspaces. *Journal of Fluid Mechanics*, 917:A18, 2021.
- Daniel Duke, Julio Soria, and Damon Honnery. An error analysis of the dynamic mode decomposition. *Experiments in fluids*, 52:529–542, 2012.

- Shervin Bagheri. Effects of weak noise on oscillating flows: Linking quality factor, floquet modes, and Koopman spectrum. *Physics of Fluids*, 26(9), 2014.
- Miguel Lázaro-Gredilla and Michalis K Titsias. Variational heteroscedastic Gaussian process regression. In *ICML*, pages 841–848, 2011.
- Andrew McHutchon and Carl Rasmussen. Gaussian process training with input noise. *Advances in neural information processing systems*, 24, 2011.
- Maziar S Hemati, Clarence W Rowley, Eric A Deem, and Louis N Cattafesta. De-biasing the dynamic mode decomposition for applied Koopman spectral analysis of noisy datasets. *Theoretical and Computational Fluid Dynamics*, 31:349–368, 2017.
- Lijian Jiang and Ningxin Liu. Correcting noisy dynamic mode decomposition with Kalman filters. *Journal of Computational Physics*, 461:111175, 2022.
- Isabel Scherl, Benjamin Strom, Jessica K Shang, Owen Williams, Brian L Polagye, and Steven L Brunton. Robust principal component analysis for modal decomposition of corrupt fluid flows. *Physical Review Fluids*, 5(5):054401, 2020.
- Taku Nonomura, Hisaichi Shibata, and Ryoji Takaki. Extended Kalman filter based dynamic mode decomposition for simultaneous system identification and denoising. *PLoS ONE*, 14(2):1–46, 02 2019. doi: 10.1371/journal.pone.0209836. URL <https://doi.org/10.1371/journal.pone.0209836>.
- Robert B Gramacy and Herbert KH Lee. Cases for the nugget in modeling computer experiments. *Statistics and Computing*, 22:713–722, 2012.
- Bernhard Schölkopf, Ralf Herbrich, and Alex J Smola. A generalized representer theorem. In *International conference on computational learning theory*, pages 416–426. Springer, 2001.
- Ciyu Zhu, Richard H Byrd, Peihuang Lu, and Jorge Nocedal. Algorithm 778: L-bfgs-b: Fortran subroutines for large-scale bound-constrained optimization. *ACM Transactions on mathematical software (TOMS)*, 23(4):550–560, 1997.
- Edward Snelson and Zoubin Ghahramani. Sparse Gaussian processes using pseudo-inputs. *Advances in neural information processing systems*, 18, 2005.
- Joaquin Quinonero-Candela and Carl Edward Rasmussen. A unifying view of sparse approximate Gaussian process regression. *The Journal of Machine Learning Research*, 6:1939–1959, 2005.
- Thang D Bui, Josiah Yan, and Richard E Turner. A unifying framework for Gaussian process pseudo-point approximations using power expectation propagation. *Journal of Machine Learning Research*, 18(104):1–72, 2017.
- Michael E Tipping. Sparse Bayesian learning and the relevance vector machine. *Journal of machine learning research*, 1(Jun):211–244, 2001.
- David R Hardoon, Sandor Szedmak, and John Shawe-Taylor. Canonical correlation analysis: An overview with application to learning methods. *Neural computation*, 16(12):2639–2664, 2004.
- Ali Rahimi and Benjamin Recht. Random features for large-scale kernel machines. *Advances in neural information processing systems*, 20, 2007.
- Feliks Nüske and Stefan Klus. Efficient approximation of molecular kinetics using random fourier features. *The Journal of Chemical Physics*, 159(7), 2023.
- Thomas M Cover. *Elements of information theory*. John Wiley & Sons, 1999.
- Alexander G de G Matthews, James Hensman, Richard Turner, and Zoubin Ghahramani. On sparse variational methods and the kullback-leibler divergence between stochastic processes. In *Artificial Intelligence and Statistics*, pages 231–239. PMLR, 2016.
- Christopher Williams and Matthias Seeger. Using the Nyström method to speed up kernel machines. *Advances in neural information processing systems*, 13, 2000.

- Igor Mezić. Spectral properties of dynamical systems, model reduction and decompositions. *Nonlinear Dynamics*, 41:309–325, 2005.
- Krikamol Muandet, Kenji Fukumizu, Bharath Sriperumbudur, and Bernhard Schölkopf. Kernel mean embedding of distributions: A review and beyond. *Foundations and Trends in Machine Learning*, 10(1-2):1 – 141, 2017. doi: 10.1561/22000000060. Cited by: 286; All Open Access, Green Open Access.
- Bernhard Schölkopf, Alexander Smola, and Klaus-Robert Müller. Nonlinear component analysis as a kernel eigenvalue problem. *Neural computation*, 10(5):1299–1319, 1998.
- Bernhard Schölkopf, Alexander Smola, and Klaus-Robert Müller. Kernel principal component analysis. In *International conference on artificial neural networks*, pages 583–588. Springer, 1997.
- Sebastian Mika, Bernhard Schölkopf, Alex Smola, Klaus-Robert Müller, Matthias Scholz, and Gunnar Rätsch. Kernel pca and de-noising in feature spaces. *Advances in neural information processing systems*, 11, 1998.
- Francis R Bach and Michael I Jordan. Kernel independent component analysis. *Journal of machine learning research*, 3(Jul):1–48, 2002.
- Kenji Fukumizu, Francis R Bach, and Arthur Gretton. Statistical consistency of kernel canonical correlation analysis. *Journal of Machine Learning Research*, 8(2), 2007.
- Igor Mezić and Andrzej Banaszuk. Comparison of systems with complex behavior. *Physica D: Nonlinear Phenomena*, 197(1-2):101–133, 2004.
- Hassan Arbabi and Igor Mezić. Study of dynamics in post-transient flows using Koopman mode decomposition. *Physical Review Fluids*, 2(12):124402, 2017.
- Jérémy Basley, LR Pastur, François Lusseyran, Th M Faure, and Nathalie Delprat. Experimental investigation of global structures in an incompressible cavity flow using time-resolved piv. *Experiments in Fluids*, 50:905–918, 2011.
- Le Song, Jonathan Huang, Alex Smola, and Kenji Fukumizu. Hilbert space embeddings of conditional distributions with applications to dynamical systems. In *Proceedings of the 26th Annual International Conference on Machine Learning, ICML ’09*, page 961–968, New York, NY, USA, 2009. Association for Computing Machinery. ISBN 9781605585161. doi: 10.1145/1553374.1553497. URL <https://doi.org/10.1145/1553374.1553497>.
- Sayak Ray Chowdhury and Aditya Gopalan. On kernelized multi-armed bandits. In *International Conference on Machine Learning*, pages 844–853. PMLR, 2017.
- Sayak Ray Chowdhury and Rafael Oliveira. Value function approximations via kernel embeddings for no-regret reinforcement learning. In Emtiyaz Khan and Mehmet Gonen, editors, *Proceedings of The 14th Asian Conference on Machine Learning*, volume 189 of *Proceedings of Machine Learning Research*, pages 249–264. PMLR, 12–14 Dec 2023. URL <https://proceedings.mlr.press/v189/chowdhury23a.html>.
- Le Song, Kenji Fukumizu, and Arthur Gretton. Kernel embeddings of conditional distributions: A unified kernel framework for nonparametric inference in graphical models. *IEEE Signal Processing Magazine*, 30(4):98–111, 2013. doi: 10.1109/MSP.2013.2252713.
- Benyamin Ghogh, Ali Ghodsi, Fakhri Karray, and Mark Crowley. Reproducing kernel Hilbert space, Mercer’s theorem, eigenfunctions, Nyström method, and use of kernels in machine learning: Tutorial and survey. *arXiv preprint arXiv:2106.08443*, 2021.
- J. Diestel and J.J. Uhl. *Vector Measures*. Mathematical surveys and monographs. American Mathematical Society, 1977. ISBN 9780821815151. URL <https://books.google.de/books?id=fEKZAwAAQBAJ>.
- Kenji Fukumizu, Francis R Bach, and Michael I Jordan. Dimensionality reduction for supervised learning with reproducing kernel Hilbert spaces. *Journal of Machine Learning Research*, 5(Jan):73–99, 2004.

- Bharath K Sriperumbudur, Arthur Gretton, Kenji Fukumizu, Gert Lanckriet, and Bernhard Schölkopf. Injective Hilbert space embeddings of probability measures. In *21st Annual Conference on Learning Theory (COLT 2008)*, pages 111–122. Omnipress, 2008.
- Charles R Baker. Joint measures and cross-covariance operators. *Transactions of the American Mathematical Society*, 186:273–289, 1973.
- Kenji Fukumizu, Le Song, and Arthur Gretton. Kernel Bayes’ rule: Bayesian inference with positive definite kernels. *The Journal of Machine Learning Research*, 14(1):3753–3783, 2013.
- Andrey Nikolayevich Tikhonov. Solutions of ill-posed problems. *VH Winston and Sons*, 1977.
- Gary Froyland, Simon Lloyd, and Naratip Santitissadeekorn. Coherent sets for nonautonomous dynamical systems. *Physica D: Nonlinear Phenomena*, 239(16):1527–1541, 2010.
- Stefan Klus, Brooke E Husic, Mattes Mollenhauer, and Frank Noé. Kernel methods for detecting coherent structures in dynamical data. *Chaos: An Interdisciplinary Journal of Nonlinear Science*, 29(12), 2019.
- Frank Noé and Cecilia Clementi. Kinetic distance and kinetic maps from molecular dynamics simulation. *Journal of chemical theory and computation*, 11(10):5002–5011, 2015.

Appendix A Gaussian Process Regression

Given a *training data set* $\mathcal{D} = \{(\mathbf{x}_i, y_i)\}_{i=1}^N$ consisting of N pairs of D -dimensional *inputs* (covariates) and scalar *outputs* (targets or dependent variables), the goal is to estimate the distribution of the function evaluation $f(\mathbf{x}_*)$ at any novel *test* location $\mathbf{x}_* \in \mathbb{X}$, where $f: \mathbb{X} \rightarrow \mathbb{R}$.

We start by grouping the inputs and outputs into the data matrices $\mathbf{X} := [\mathbf{x}_1, \dots, \mathbf{x}_N] \in \mathbb{R}^{D \times N}$ and $\mathbf{Y} := [y_1, \dots, y_N] \in \mathbb{R}^{1 \times N}$. Note that while GP regression supports a wide variety of input domains, we have defined $\mathbb{X} \subseteq \mathbb{R}^D$.

Our first modeling assumption is that the sensor noise on the targets is additive, independent, and Gaussian. Consequently, the relationship between the input random variable X and the output random variable Y is

$$Y_i = f(X_i) + \epsilon_i, \quad \text{where } \epsilon_i \sim \mathcal{N}(0, \sigma_Y^2), \quad (\text{A.1})$$

and σ_Y^2 is the homoscedastic variance of the sensor noise or the *nugget* term for surrogate mismodeling [Gramacy and Lee, 2012].

A.1 Reproducing Kernel Hilbert Spaces

A reproducing kernel $\kappa: \mathbb{X} \times \mathbb{X} \rightarrow \mathbb{R}$ is a bivariate positive semidefinite function. A rough sketch of the role of a kernel function is as a measure of the *similarity* (or affinity) between two inputs, \mathbf{x} and \mathbf{x}' . This notion of ‘similarity’ is expressed through an inner product between the embeddings of the two inputs into a reproducing kernel Hilbert space (RKHS), \mathbb{H} [Berlinet and Thomas-Agnan, 2011]. This inner product is embodied by the *kernel trick*:

$$\kappa(\mathbf{x}, \mathbf{x}') = \langle \kappa(\mathbf{x}, \cdot), \kappa(\mathbf{x}', \cdot) \rangle_{\mathbb{H}}.$$

The kernel trick encapsulates the properties that make RKHS methods so effective. All kernel functions are constructed through the *Riesz representation theorem* [Hsing and Eubank, 2015, Fréchet, 1904, Schölkopf et al., 2001], such that the *reproducing property* $f(\mathbf{x}) = \langle f, \kappa(\mathbf{x}, \cdot) \rangle_{\mathbb{H}} \forall f \in \mathbb{H}$ is satisfied *twice* over. What this means will become clear shortly. First define the *feature map* $\varphi: \mathbb{X} \rightarrow \mathbb{H}$ according to $\varphi(\mathbf{x}) := \kappa(\mathbf{x}, \cdot) \in \mathbb{H}$. Now consider that the reproducing property allows us to evaluate any function in \mathbb{H} . What this implies, is that since both $\varphi(\mathbf{x})$ and $\varphi(\mathbf{x}')$ are both elements of \mathbb{H} , they act as the evaluation functionals of the other.

Alternatively, one may think of any two points $\mathbf{x}, \mathbf{x}' \in \mathbb{X}$ as vertices on a symmetric graph where the weight of the edge connecting them, $\kappa(\mathbf{x}, \mathbf{x}')$, is a quantitative comparison between two more complex objects. In this sense, a reproducing kernel defines a local geometry on \mathbb{X} . The practical benefit of the feature map is that while the input data may have very few discernible structures, we can represent more nonlinear structures with $\varphi(\cdot)$.

A.2 Bayes’ Law

Informally, *Gaussian processes* (GPs) are mathematical objects that are generalizations of multivariate normal distributions. Recall that a multivariate normal distribution describes random variables that are vectors of *finite* dimensionality. If the input domain were real numbers, then roughly speaking the random variable described by a GP is a “vector” of *infinite* dimensionality indexed not by a natural number but by a real number. More formally, according to the *function-space view*, a GP represents a probability distribution over $f \in \mathbb{H}$.

GP regression proceeds following a *Bayesian* philosophy, which identifies the *likelihood* with the probability density $p_{\text{om}}(y_i | f, \mathbf{x}_i) = \mathcal{N}(y_i; f(\mathbf{x}_i), \sigma_Y^2)$. As indicated by the subscript, the likelihood captures the *observation model*, i.e., the probabilistic mapping between a noise-free latent function evaluation and the noisy target. The likelihood tells us how to update our prior beliefs of the regression function with new data.

It follows that the next step is placing a GP *prior* over the function $f(\cdot)$ such that $p_{\text{pr}}(f) = \mathcal{GP}(f; m_{\text{pr}}(\cdot), \kappa_{\text{pr}}(\cdot, \cdot))$. Here $m_{\text{pr}}: \mathbb{X} \rightarrow \mathbb{R}$ is the prior mean function $\mathbb{E}[f(\cdot)]$. The second component of the GP prior, the reproducing kernel $\kappa_{\text{pr}}(\mathbf{x}, \mathbf{x}')$, encodes $\mathbb{E}[(f(\mathbf{x}) - m_{\text{pr}}(\mathbf{x}))(f(\mathbf{x}') - m_{\text{pr}}(\mathbf{x}'))]$, i.e., the prior covariance between function values.

The combination of the likelihood and the prior defines the *generative model*. Accordingly, we refer to θ as the set of *generative* hyperparameters, which parameterize both the prior kernel function $\kappa_{\text{pr}}(\cdot, \cdot)$ and the characteristics of the sensor noise. To lighten the notation, we may omit the dependence of the probability densities on θ .

An important feature, is that a GP evaluated on the finite subset $\{\mathbf{x}_i\}_{i=1}^N \subset \mathbb{X}$ is an N -dimensional multivariate Gaussian random variable. Without loss of generality, if we choose a GP prior with a mean function that is identically zero $m_{\text{pr}} \equiv 0$, then a priori the function values will behave according to the distribution,

$$p_{\text{pr}}(\mathbf{f}_X) = \mathcal{N}^N(\mathbf{f}_X; \mathbf{0}, \mathbf{K}_{XX}),$$

where we have introduced two new variables that are best understood at hand of the *dictionary*:

$$\Phi_X := [\varphi(\mathbf{x}_1) \quad \dots \quad \varphi(\mathbf{x}_N)] \in \mathbb{H}^{1 \times N}.$$

In essence, the dictionary collects the lifting functions and is a generalization of the *design matrix* in linear regression.

The adjoint of the dictionary operator is called the *observation operator*, since $\Phi_X^\top : \mathbb{H} \rightarrow \mathbb{R}^N$ is a mapping from the feature space to the observable space. By the reproducing property, the observation operator allows us to sample a function $f \in \mathbb{H}$. Therefore, we can define the vector of latent function values as $\mathbf{f}_X := \Phi_X^\top f = [f(\mathbf{x}_1), \dots, f(\mathbf{x}_N)]^\top$, and the *variance-covariance matrix* by $\mathbf{K}_{XX} := [\kappa_{\text{pr}}(\mathbf{x}_i, \mathbf{x}_j)]_{i,j=1}^N = \kappa_{\text{pr}}(\mathbf{X}, \mathbf{X}) = \Phi_X^\top \Phi_X$. Simply put, GPs treat every latent function value as a random variable.

The final product of a GP model is the conditional probability density of novel function evaluations [Rasmussen and Williams, 2006]. This posterior predictive distribution can be inferred via Bayes' rule, the prior GP (over both training and test latent values), and the likelihood. Should we assume that the training data set is i.i.d., then the likelihood factorizes over all N samples, and the exact posterior process over $f(\cdot)$ can be expressed as

$$p_{\text{pst}}(f | \mathcal{D}) = \frac{\prod_{i=1}^N p_{\text{om}}(y_i | f(\mathbf{x}_i)) p_{\text{pr}}(f)}{\int \prod_{i=1}^N p_{\text{om}}(y_i | f(\mathbf{x}_i)) p_{\text{pr}}(f) df}.$$

Because the likelihood was Gaussian to begin with, the posterior process is also a GP admitting a closed-form expression. To derive this expression, we marginalize out the latent function values at the training points, resulting in a posterior distribution that is fully specified by

$$m_{\text{pst}}(\mathbf{x}) := \mathbf{A} \mathbf{k}_X(\mathbf{x}), \quad (\text{A.2})$$

$$\kappa_{\text{pst}}(\mathbf{x}, \mathbf{x}') := \kappa_{\text{pr}}(\mathbf{x}, \mathbf{x}') - \mathbf{k}_X^\top(\mathbf{x}) \tilde{\mathbf{K}}_{XX}^{-1} \mathbf{k}_X(\mathbf{x}'), \quad (\text{A.3})$$

where $\mathbf{A} := \mathbf{Y} \tilde{\mathbf{K}}_{XX}^{-1} \in \mathbb{R}^{1 \times N}$ is the *weight matrix*, $\tilde{\mathbf{K}}_{XX} := \mathbf{K}_{XX} + \sigma_Y^2 \mathbf{I}_N$ is the covariance matrix for the noisy outputs⁶, and $\mathbf{k}_X(\mathbf{x}) := \Phi_X^\top \varphi(\mathbf{x}) = [\kappa_{\text{pr}}(\mathbf{x}_1, \mathbf{x}), \dots, \kappa_{\text{pr}}(\mathbf{x}_N, \mathbf{x})]^\top$ is a *feature vector*. Now, all our questions about the *noisy* predictive posterior distribution at some unseen input \mathbf{x}_* can be answered by querying the expression:

$$p_{\text{pst}}(y_* | \mathcal{D}) = \mathcal{N}(y_*; m_{\text{pst}}(\mathbf{x}_*), \kappa_{\text{pst}}(\mathbf{x}_*, \mathbf{x}_*) + \sigma_Y^2).$$

Since the quality of the posterior solution is sensitive to θ , it is typically prudent to first attempt to infer the optimal hyperparameters, θ^* . The denominator in Bayes' rule, $p_{\text{ml}}(\mathbf{Y})$, known as *marginal likelihood* (or *evidence*) paves a path to craft an optimization algorithm for model selection, since it takes into account the entire generative model. In other words, it is natural to choose θ^* , such that it maximizes the probability of observing the targets given the model's posterior function evaluations. To this end, the closed-form expression for the log-marginal likelihood is

$$\begin{aligned} \ln(p_{\text{ml}}(\mathbf{Y})) &= \ln \left(\int p_{\text{om}}(\mathbf{Y} | \mathbf{f}_X) p_{\text{pr}}(\mathbf{f}_X) d\mathbf{f}_X \right) \\ &= -\frac{1}{2} \left[\underbrace{N \ln(2\pi)}_{\text{constant}} + \underbrace{\ln(|\tilde{\mathbf{K}}_{XX}|)}_{\text{model complexity}} + \underbrace{\mathbf{Y} \tilde{\mathbf{K}}_{XX}^{-1} \mathbf{Y}^\top}_{\text{data mismatch}} \right]. \end{aligned} \quad (\text{A.4})$$

Maximizing (A.4) naturally embodies Occam's razor, and can be interpreted as engineering the prior GP such that it maximizes the volume of data-matching functions.⁷

⁶The *noise kernel* models a constant covariance over the state space \mathbb{X} with $\kappa_\sigma(\mathbf{x}, \mathbf{x}') := \sigma^2 \delta(\mathbf{x}, \mathbf{x}')$, which is a scaled Kronecker delta function. Couple this with the fact that the sum of kernel functions is a valid kernel.

⁷One can often find an analytical expression for the gradient of (A.4) and use optimization algorithms such as conjugate gradient ascent or BFGS [Zhu et al., 1997].

A.3 Sparse Regression

The most salient downside of GP regression is the computational complexity of identifying the posterior. Computing the exact posterior GP in conventional GP regression requires the inversion of an $N \times N$ matrix, which takes $\mathcal{O}(N^3)$ runtime, and $\mathcal{O}(N^2)$ memory space to store the weights and the training inputs. The cubic time-complexity and quadratic memory consumption create a bottleneck that hinders GPs from being deployed on data sets larger than a few thousand points.

To mitigate these computational drawbacks, practitioners resort to approximation techniques that employ an additional smaller *pseudo-data set*. This data set is comprised of *pseudo-outputs* (i.e., inducing variables) $\mathbf{f}_Z = \Phi_Z^\top f$ that are unknown evaluations of the *pseudo-inputs* (i.e., inducing inputs or points) $\mathbf{Z} := \{\mathbf{z}_i \in \mathbb{X}\}_{i=1}^M$. Such pseudo-data set schemes are widely used to reduce a kernel-based algorithm's training time-complexity to $\mathcal{O}(NM^2)$ and the memory-complexity to $\mathcal{O}(NM)$ [Snelson and Ghahramani, 2005, Quinonero-Candela and Rasmussen, 2005, Bui et al., 2017]. The variable M , representing the cardinality of the pseudo-data set, governs the expressiveness of the sparse GP. The pseudo-inputs, \mathbf{Z} , play a similar role in support or relevance vector machines [Schölkopf and Smola, 2002, Tipping, 2001].⁸

The challenge now becomes to construct an expression for the sparse posterior and jointly infer the hyperparameters and the pseudo-inputs. One approach is to design the approximated posterior GP so that it is as close as possible to the true posterior GP. The phrase "as close as possible" can be, for example, interpreted as minimizing the *Kullback–Leibler* (KL) divergence between the sparse posterior GP and the exact posterior GP [Cover, 1999]. This particular optimization objective is explored in the *variational free energy* (VFE) method of [Titsias, 2009].

In variational inference of GPs a distribution $q(f)$ is introduced over the entire infinite-dimensional function f as an approximation to $p_{\text{pst}}(f | \mathcal{D})$. The primary advantage of the VFE framework is that the pseudo-inputs are treated as *variational* parameters of an approximated posterior rather than as generative parameters. These variational parameters are automatically protected from overfitting, since the optimization is between the exact posterior and an approximated posterior. In other words, the variational parameters are resilient against assumptions about the generative model [Lázaro-Gredilla and Titsias, 2011]. Another advantage of the VFE method is that increasing M is guaranteed to monotonically improve the approximation.

Definition A.1. The *variational free energy* (VFE; Matthews et al. [2016]):

$$\mathcal{F}(\theta, \mathbf{Z}) := \int \ln \left(\frac{p(\mathbf{Y}, f | \theta)}{q(f)} \right) q(f) \, df \leq \ln(p_{\text{ml}}(\mathbf{Y})),$$

is often referred to as the *evidence lower bound* (ELBO).

Under the i.i.d. data assumption, the VFE can be written as

$$\begin{aligned} \mathcal{F}(\theta, \mathbf{Z}) &= \sum_{i=1}^N \int \ln(p_{\text{om}}(y_i | f_i, \theta)) q(f_i | \theta) \, df_i \\ &\quad - KL(q(\mathbf{f}_Z) || p_{\text{pr}}(\mathbf{f}_Z | \theta)), \end{aligned}$$

where $q(\mathbf{f}_Z)$ is a free-form multivariate Gaussian distribution, and $p_{\text{pr}}(\mathbf{f}_Z | \theta) = \mathcal{N}^M(\mathbf{f}_Z; \mathbf{0}, \mathbf{K}_{ZZ})$ refers to the prior Gaussian distribution over the pseudo-outputs \mathbf{f}_Z .

Due to the Gaussian assumptions, the calculus of variations can be used to analytically solve for the optimal approximate posterior Gaussian process. This results in the following posterior mean and covariance functions:

$$m_{\text{pst}}(\mathbf{x}) := \mathbf{A} \mathbf{k}_Z(\mathbf{x}), \tag{A.5}$$

$$\kappa_{\text{pst}}(\mathbf{x}, \mathbf{x}') := \kappa_{\text{pr}}(\mathbf{x}, \mathbf{x}') - \mathbf{k}_Z^\top(\mathbf{x}) \tilde{\mathbf{B}} \mathbf{k}_Z(\mathbf{x}'). \tag{A.6}$$

Here, we are deviating from the notation in [Titsias, 2009] to highlight the similarities with (kernel) ridge-regression. The *weight matrix*, $\mathbf{A} := \mathbf{Y} \mathbf{K}_{ZX}^\top \tilde{\mathbf{C}}_{XX}^{-1}$, contains the regression coefficients obtained from linear operations on matrices. The noisy *Gramian* is defined by $\tilde{\mathbf{C}}_{XX} := \mathbf{K}_{ZX} \mathbf{K}_{ZX}^\top + \sigma_Y^2 \mathbf{K}_{ZZ}$, and

⁸Speed-ups can also be realized through low-rank methods, such as partial Gram–Schmidt orthogonalization [Shawe-Taylor, 2004, Hardoon et al., 2004], random Fourier features [Rahimi and Recht, 2007, Nüske and Klus, 2023], or the LASSO-like algorithm of [Grünewälder et al., 2012].

the *cross-covariance* matrix by $\mathbf{K}_{ZX} := \kappa_{\text{pr}}(\mathbf{Z}, \mathbf{X}) \in \mathbb{R}^{M \times N}$. Lastly, to compute the posterior kernel the weights for the *information gain* term are $\tilde{\mathbf{B}} := (\mathbf{K}_{ZZ}^{-1} - \sigma_Y^2 \tilde{\mathbf{C}}_{XX}^{-1})$.

The VFE, i.e., the quantity that we maximize, is

$$\mathcal{F}(\theta, \mathbf{Z}) = \ln(\mathcal{N}^N(\mathbf{Y}; \mathbf{0}, \tilde{\mathbf{R}})) - \frac{1}{2\sigma_Y^2} \text{Tr}(\mathbf{K}_{XX} - \mathbf{R}), \quad (\text{A.7})$$

where $\mathbf{R} := \mathbf{K}_{ZX}^\top \mathbf{K}_{ZZ}^{-1} \mathbf{K}_{ZX}$ is the *Nyström approximation* to the exact prior covariance matrix, and $\tilde{\mathbf{R}} := \mathbf{R} + \sigma_Y^2 \mathbf{I}_N$ is its noisy variant [Williams and Seeger, 2000]. Notice that the closed-form expression in (A.7) is very similar to that of the exact log-marginal likelihood (A.4), with the addition of the trace term. The trace term encourages pseudo-inputs to better capture the training data, and is proportional to the sum of the variances of the training function values given the pseudo-targets, $p(\mathbf{f}_X | \mathbf{f}_Z)$, i.e., the total squared error of predicting \mathbf{f}_X given \mathbf{f}_Z .

Appendix B Transfer Operator Theory

GP regression as presented in Appendix A can directly be applied to time-series data. However, if we merge GP regression with transfer operator theory we can efficiently perform multi-step predictions and, as advertised earlier, gain a deeper understanding of the dynamical system.

To that end, we proceed by recalling the definition of the Koopman operator for random dynamical systems (RDSs), specifically for stationary and ergodic Markov processes [Klus et al., 2016, Črnjarić-Zic et al., 2020]. These include, for example, stochastic differential equations driven by Gaussian white noise and discrete systems generated by i.i.d. random maps.

Consider the continuous-time stochastic dynamical systems represented by the time-homogeneous Itô stochastic differential equation (SDE),

$$d\mathbf{x}_t = \mathbf{r}(\mathbf{x}_t) dt + \mathbf{h}(\mathbf{x}_t) dW_t, \quad t \geq 0, \quad (\text{B.1})$$

where $\{\mathbf{x}_t\}_{t \geq 0}$ is a stochastic process defined on the state space \mathbb{X} , and W_t is the D -dimensional standard Wiener process (i.e., Brownian motion). Such stochastic dynamics arise when there is process noise present in the system, which enters in the form of a diffusion term $\mathbf{h}(\mathbf{x}_t)$. The first term $\mathbf{r}(\mathbf{x}_t)$, is commonly referred to as the friction or drift term. Both $\mathbf{h}: \mathbb{X} \rightarrow \mathbb{X}$ and $\mathbf{r}: \mathbb{X} \rightarrow \mathbb{X}$ are assumed to be smooth time-invariant nonlinear vector fields.

While Koopman theory covers continuous-time dynamics, we convert to discrete-time dynamics by sampling trajectories at uniform time intervals, Δt , such that $t_k := \Delta t k$, which implies $t_k + \Delta t = t_{k+1}$, $\forall k \in \mathbb{N}$. The resulting discrete-time Markov process can be represented by the *flow map* $\mathbf{F}_\alpha: \mathbb{X} \rightarrow \mathbb{X}$, which is indexed by the random variable $\alpha \in \Omega$ such that $Y = \mathbf{F}_\alpha(X)$, where Ω is the probability space associated with the stochastic dynamics. The resulting discrete-time RDS, possesses a *transition density function*, $p_{\Delta t}: \mathbb{X} \times \mathbb{X} \rightarrow \mathbb{R}_{\geq 0}$, such that the expression $p_{\Delta t}(\mathbf{x}_{k+1} | \mathbf{x}_k)$ represents the conditional probability of observing the next state \mathbf{x}_{k+1} given the current state \mathbf{x}_k .

B.1 The Koopman and Perron–Frobenius Operators

The starting point for Koopman theory is mapping the RDS from the lower-dimensional nonlinear space \mathbb{X} to a higher-dimensional linear space \mathbb{G} , such that no information is lost when moving to this feature space. In short, operator theory can be viewed as a trade-off between lifting the state space into a feature space with more complex states but simpler dynamics. To perform the lifting, the literature defines an *observable* function as, $g \in \mathbb{G}$, where $\mathbb{G} = \mathcal{L}^\infty(\mathbb{X})$.⁹

Definition B.1. The *stochastic Koopman operator* (SKO) [Williams et al., 2015a, Mezić, 2005] $\mathcal{U}: \mathbb{G} \rightarrow \mathbb{G}$ is defined as the conditional expectation of any observable composed with the flow,

$$\begin{aligned} (\mathcal{U}g)(\mathbf{x}) &= \mathbb{E}[g(Y) | X = \mathbf{x}] \\ &= \int p_{\Delta t}(\mathbf{y} | \mathbf{x}) g(\mathbf{y}) d\mathbf{y}. \end{aligned}$$

In general, an observable may be a vector-valued function, $\mathbf{g} \in \mathbb{G}^P$. Of particular interest is the *full-state observable*, $\mathbf{g}(\mathbf{x}) = \mathbf{x}$, and the *extended-state observable*, $\mathbf{g}(\mathbf{x}) = \mathbf{k}_X(\mathbf{x})$. From a theoretical perspective, we often only consider scalar-valued observables, $g: \mathbb{X} \rightarrow \mathbb{R}$, and have \mathcal{U} act component-wise on the set of observables $\{g_i\}_{i=1}^P$.

⁹Other Banach spaces for \mathbb{G} are also valid, e.g., the Hilbert space of Lebesgue square-integrable functions, i.e., $\mathbb{G} := L^2(\mathbb{X})$ [Ikeda et al., 2022, Klus et al., 2020b].

Definition B.2. The *Perron–Frobenius operator* (PFO) is concerned with an ensemble of trajectories and acts on the conjugate space of probability densities $\mathcal{P} : \mathcal{L}^1(\mathbb{X}) \rightarrow \mathcal{L}^1(\mathbb{X})$:

$$(\mathcal{P}p)(\mathbf{y}) = \int p_{\Delta t}(\mathbf{y} | \mathbf{x}) p(\mathbf{x}) d\mathbf{x}.$$

Hence we call any operator, transporting some object (a distribution, or an observable) by the dynamics, a transfer operator, i.e., the action of the process on functions of the state. The mathematical formulations of *kernel* transfer operators follow from the assumptions that the observables are elements of an RKHS feature space, and the operators are compact with a discrete spectrum [Klus *et al.*, 2020b]. This implies that we may set $\mathbb{G} = \mathbb{H}$.

Strictly speaking, the definitions of kernel transfer operators are formulated in the language of kernel mean embeddings (KMEs) [Muandet *et al.*, 2017]. KME is another statistical learning theory, which typically falls within the *frequentist* paradigm. KME is closely associated with kernel principal component analysis (KPCA) and kernel canonical correlation analysis (KCCA), both of which are considered to be unsupervised learning techniques [Hardoon *et al.*, 2004, Schölkopf *et al.*, 1998, 1997, Mika *et al.*, 1998, Bach and Jordan, 2002, Fukumizu *et al.*, 2007]. For the sake of completeness, the theory describing KMEs is recapitulated in Appendix C.

B.2 Koopman Mode Decomposition

The crux of transfer operator analysis rests upon the fact that the nonlinear dynamics are linear in the eigenfunction coordinates [Mauroy *et al.*, 2020]. These *eigenfunctions* $\{\phi_i \in \mathbb{G}\}_{i=1}^{\infty}$, and the corresponding *eigenvalues* $\{\lambda_i \in \mathbb{C}\}_{i=1}^{\infty}$, of \mathcal{U} , obey the following equation in discrete time:

$$\phi_i(\mathbf{x}_{k+1}) = \mathcal{U}\phi_i(\mathbf{x}_k) = \lambda_i\phi_i(\mathbf{x}_k). \quad (\text{B.2})$$

Assuming that the dynamical systems we are dealing with have discrete point spectra, the evolution of the observables can be expanded in terms of the eigenfunctions and the eigenvalues. Specifically we can write the infinite series:

$$(\mathcal{U}\mathbf{g})(\mathbf{x}) = \sum_{i=1}^{\infty} \mathbf{v}_i \lambda_i \phi_i(\mathbf{x}),$$

which is a generalization of the Sturm–Liouville expansion for a differential problem.

Every *Koopman mode*, $\mathbf{v}_i \in \mathbb{C}^P$, is determined by the dictionary of observables and is associated with an eigenpair (λ_i, ϕ_i) . The modes are in essence the coefficients used to construct $\mathbf{g}(\cdot)$ using the Koopman eigenfunction basis. In other words, the observables can be expanded into a weighted sum of eigenfunctions:

$$\mathbf{g} = \sum_{i=1}^{\infty} \mathbf{v}_i \phi_i \in \mathbb{G}^P.$$

Altogether, the modes and eigenpairs allow us to reconstruct and propagate the system’s state arbitrarily far into the future [Williams *et al.*, 2015a]. Where the eigenvalues describe the temporal behavior of the dynamical system, the modes capture the spatial behavior. Once we have found the sequence of triplets $\{(\lambda_i, \phi_i, \mathbf{v}_i)\}_{i=1}^{\infty}$ for a dynamical system, we have completed its *Koopman mode decomposition* (KMD; Mezić [2005], Mezić and Banaszuk [2004]).

B.3 Finite-Dimensional Approximation

The challenge is that the Koopman operator is infinite-dimensional. As far as numerical methods are concerned, we want to find a reduced but finite set $\{(\lambda_i, \phi_i, \mathbf{v}_i)\}_{i=1}^M$, such that the evolution of all observable functions can be reasonably well approximated. That is, the goal is to derive a matrix representation of the SKO by projecting it onto a finite-dimensional subspace, such that a finite-dimensional linear system is induced [Colbrook and Townsend, 2024].

The matrix representation of the transfer operator can be obtained by restricting the operator to an *invariant subspace*. Note that when the Koopman operator of a dynamical system has a continuous eigenvalue spectrum, as is the case for chaotic systems, the discretization will be flawed [Arbabi and Mezić, 2017, Basley *et al.*, 2011].

The subspace spanned by the elements of Φ_Z , $\mathbb{G}_M := \text{span}\{\Phi_Z\}$, is *invariant* if all observables $g \in \mathbb{G}_M$ can be written as a linear combination of the dictionary functions,

$$g = \sum_{i=1}^M q_i \varphi(\mathbf{z}_i) = \Phi_Z \mathbf{q}, \quad \mathbf{q} \in \mathbb{R}^M,$$

and they remain in this subspace after acted upon by the Koopman operator, i.e., $\mathcal{U}g \in \mathbb{G}_M$ [Williams *et al.*, 2015a].

On route to a finite-dimensional matrix representation, we define a bounded linear map $\Gamma_Z: \mathbb{G} \rightarrow \mathbb{R}^M$ that yields the coordinates of an observable in the basis $\{\varphi(\mathbf{z}_i)\}_{i=1}^M$. Applying Γ_Z to an observable $g \in \mathbb{G}$ returns the coefficients, $\mathbf{q} = \Gamma_Z g \in \mathbb{R}^M$. In turn, having the dictionary operator act on \mathbf{q} , will recover the best approximation to the observable in \mathbb{G}_M , $\Phi_Z \mathbf{q} = \Pi_Z g \approx g$, where $\Pi_Z := \Phi_Z \Gamma_Z$. For an invariant subspace, it is evident that Π_Z commutes with \mathcal{U} , which implies that $\Gamma_Z \Phi_Z = \mathbf{I}_M$, and hence $\mathbb{G} = \mathbb{G}_M$.

Altogether the compression of the Koopman operator to the subspace $\mathcal{U}_M: \mathbb{G} \rightarrow \mathbb{G}_M$ is

$$\mathcal{U}_M := \Pi_Z \mathcal{U} = \Phi_Z \Gamma_Z \mathcal{U}.$$

From here we can define the finite-dimensional matrix representation $\mathbf{U}: \mathbb{R}^M \rightarrow \mathbb{R}^M$ of \mathcal{U} s.t.

$$\mathcal{U}_M g = \Pi_Z \mathcal{U} \Pi_Z g = \Phi_Z \mathbf{U} \Gamma_Z g, \quad g \in \mathbb{G},$$

which defines the *Koopman matrix* as

$$\mathbf{U} := \Gamma_Z \mathcal{U} \Phi_Z \in \mathbb{R}^{M \times M}. \quad (\text{B.3})$$

Several well-known results relate the spectral properties of the Koopman matrix \mathbf{U} to those of the operator \mathcal{U} . For example, we can decompose the eigenfunctions $\{\phi_i\}_{i=1}^M$ with

$$\phi_i = \sum_{j=1}^M w_{ij} \varphi(\mathbf{z}_j) = \Phi_Z \mathbf{w}_i, \quad \mathbf{w}_i \in \mathbb{C}^M,$$

and then apply the relationship between eigenvalues and eigenfunctions (B.2):

$$\begin{aligned} \mathcal{U}_M \phi_i &= \lambda_i \phi_i, \\ \Phi_Z \mathbf{U} \Gamma_Z \phi_i &= \lambda_i \Phi_Z \Gamma_Z \phi_i, \\ \mathbf{U} \Gamma_Z \phi_i &= \lambda_i \Gamma_Z \phi_i, \\ \mathbf{U} \mathbf{w}_i &= \lambda_i \mathbf{w}_i. \end{aligned}$$

Hence, the right eigenvectors of \mathbf{U} correspond to the coordinates of the eigenfunctions in the basis of dictionary functions, and the eigenvalues of \mathbf{U} are the eigenvalues of \mathcal{U} . The left eigenvectors of \mathbf{U} are the modes of the extended-state observable, and are related to the eigenfunctionals of the dual operator to the Koopman operator [Mauroy *et al.*, 2020].

Appendix C Embedding Probability Distributions

Unlike GP regression, which treats parameters as random variables, the kernel mean embedding (KME) approach relies on repeated sampling from a population to inform on estimates of probability distributions, and treats regression as a purely *geometric* operation between vector spaces. This geometric view is a reformulation of the frequentist least-squares solution rather than an entirely separate paradigm.

From the outset, KME allows for featurization of the output variable, while GP regression is typically presented with pure scalar-valued outputs¹⁰. In other words, the output space \mathbb{Y} is not limited to $\mathbb{Y} \subseteq \mathbb{R}$ [Song *et al.*, 2009]. In contrast with (A.2) we directly model $\mathbb{E}_{Y|\mathbf{x}}[g(Y) | X = \mathbf{x}]$, $g \in \mathbb{H}_Y$. Apart from this, the mathematical formalisms for the predictive mean (A.2) and the kernel conditional mean embedding (C.2) are exactly the same, as are the predictive variance (A.3) and the Mahalanobis distance [Chowdhury and Gopalan, 2017, Chowdhury and Oliveira, 2023]. It is a case where the GP regression and KME communities, have developed overlapping tools while having different goals in mind.

A limitation of the KME approach is that it recovers only part of the structure available in GP regression: in particular, other concepts such as the marginal likelihood do not translate directly into the embedding framework.

¹⁰In this work, we bridge the gap by providing a Bayesian interpretation of $\varphi(Y)$.

C.1 Marginal Distributions

The idea of KMEs are to identify probability distributions with elements of an RKHS that fully capture their statistical features. Operationally, we map the data to an RKHS and then we compute the mean. The embeddings are not direct estimates of probability distributions, but rather representative points or elements in an RKHS. For readers interested in embedding probability distributions in RKHSs, excellent resources are [Muandet et al., 2017, Song et al., 2009, 2013].

Definition C.1. *Marginal Mean Embedding.* Let \mathbb{H}_X be an RKHS with a bounded kernel¹¹. Then the kernel mean embedding $\mu_X \in \mathbb{H}_X$ is defined as

$$\mu_X := \mathbb{E}_X [\varphi(X)] = \int_{\mathbb{X}} \varphi(\mathbf{x}) d\mathbb{P}_X(\mathbf{x}),$$

where the integral is a Bochner integral [Hsing and Eubank, 2015, Diestel and Uhl, 1977].

For a large class of kernel functions known as *characteristic kernels* [Fukumizu et al., 2004, Sriperumbudur et al., 2008], the mean embedding captures all the necessary information about the distribution \mathbb{P}_X . In other words, the mean map $\mathbb{P}_X \rightarrow \mu_X$ is injective and there is no information lost when mapping the distribution into \mathbb{H}_X .

By virtue of the reproducing property and linearity of expectation, the marginal embedding μ_X has the property that the expectation of any Hilbert space function $f \in \mathbb{H}_X$ can be evaluated as an inner product, i.e., $\mathbb{E}_X [f(X)] = \langle f, \mu_X \rangle_{\mathbb{H}_X}$.

To realize an unbiased consistent empirical estimate $\hat{\mu}_X$ of μ_X we require that the sample set be drawn independently and identically distributed (i.i.d.) from \mathbb{P}_X . The estimate of the mean embedding can then be calculated with

$$\hat{\mu}_X := \frac{1}{N} \sum_{i=1}^N \kappa(\mathbf{x}_i, \cdot).$$

C.2 Joint Distributions

The next step is to generalize to two (or more) random variables. For joint probability distributions we compute covariance operators over tensor product spaces of RKHSs [Baker, 1973].

Definition C.2. *Joint Mean Embedding.* Let (Y, X) be a joint random variable on $\mathbb{Y} \times \mathbb{X}$ with the joint distribution \mathbb{P}_{YX} . Given the characteristic kernels κ_X and κ_Y with respective RKHSs \mathbb{H}_X and \mathbb{H}_Y , where each kernel is parametrized by θ_X and θ_Y , and the associated feature maps are φ_X and φ_Y . The trace-class *variance-covariance operator* $\mathcal{C}_{XX} : \mathbb{H}_X \rightarrow \mathbb{H}_X$ and Hilbert-Schmidt *cross-covariance operator* $\mathcal{C}_{YX} : \mathbb{H}_X \rightarrow \mathbb{H}_Y$ are defined as

$$\begin{aligned} \mathcal{C}_{YX} &:= \mathbb{E}_{YX} [\varphi_{YX}(Y, X)] = \int_{\mathbb{X} \times \mathbb{Y}} \varphi_{YX}(\mathbf{y}, \mathbf{x}) d\mathbb{P}_{YX}(\mathbf{y}, \mathbf{x}), \\ \mathcal{C}_{XX} &:= \mathbb{E}_X [\varphi_X(X, X)] = \int_{\mathbb{X}} \varphi_{XX}(\mathbf{x}, \mathbf{x}) d\mathbb{P}_X(\mathbf{x}), \end{aligned}$$

where the *joint feature map* is defined according to $\varphi_{YX}(\mathbf{y}, \mathbf{x}) := \varphi_Y(\mathbf{y}) \otimes \varphi_X(\mathbf{x})$. Through the joint feature map, a pair of realizations (\mathbf{y}, \mathbf{x}) can be lifted into the tensor-product feature space $\mathbb{H}_{YX} := \mathbb{H}_Y \otimes \mathbb{H}_X$, i.e., the space of linear operators from \mathbb{H}_Y to \mathbb{H}_X .

The cross-covariance operator expresses the covariance between functions in \mathbb{H}_{YX} , and contains all the information regarding the dependencies of X and Y . If both κ_X and κ_Y are linear kernels such that the feature maps φ_X and φ_Y are identity maps, we recover the standard covariance matrices. Hence, one may think of \mathcal{C}_{XX} and \mathcal{C}_{YX} as nonlinear generalizations of these matrices. Using these ideas, the cross-covariance between two functions $f \in \mathbb{H}_X$ and $g \in \mathbb{H}_Y$ is

$$\begin{aligned} \mathbb{E}_{YX} [f(X)g(Y)] &= \langle f, \mathcal{C}_{XY}g \rangle_{\mathbb{H}_X} = \langle \mathcal{C}_{YX}f, g \rangle_{\mathbb{H}_Y} \\ &= \langle g \otimes f, \mathcal{C}_{YX} \rangle_{\mathbb{H}_{YX}}. \end{aligned}$$

¹¹Stationary kernels (functions only depending on the distance between the inputs), such as the Matérn or squared exponential kernels, are bounded $\sup_{\mathbf{x}, \mathbf{y} \in \mathbb{X}} \kappa(\mathbf{x}, \mathbf{y}) < \infty$ [Rasmussen and Williams, 2006, Ghogh et al., 2021].

Therefore, \mathcal{C}_{XX} is a self-adjoint operator and \mathcal{C}_{YX} is the adjoint of \mathcal{C}_{XY} . Note that the joint feature map is a rank one operator. Consequently, there is an interesting duality of perspectives at play, because just like the mean embedding was an element in the RKHS $\mu_X \in \mathbb{H}_X$, so the cross-covariance operator is an element in the tensor product feature space $\mathcal{C}_{YX} \in \mathbb{H}_{YX}$.

The empirical estimators for the covariance operators given i.i.d. samples $\{(\mathbf{x}_i, \mathbf{y}_i)\}_{i=1}^N$ are:

$$\begin{aligned}\hat{\mathcal{C}}_{YX} &:= \frac{1}{N} \sum_{i=1}^N \varphi_{YX}(\mathbf{y}_i, \mathbf{x}_i) = \frac{1}{N} \Phi_Y \Phi_X^\top, \\ \hat{\mathcal{C}}_{XX} &:= \frac{1}{N} \Phi_X \Phi_X^\top, \text{ and } \hat{\mathcal{C}}_{YY} := \frac{1}{N} \Phi_Y \Phi_Y^\top.\end{aligned}\tag{C.1}$$

C.3 Conditional Distributions

We are now in a position to introduce RKHS embeddings of conditional probability distributions, known as *conditional mean embeddings* (CMEs). To do so, we require the following result, which relates the two operators \mathcal{C}_{XX} and \mathcal{C}_{XY} .

Proposition C.3. *If $\mathbb{E}_{Y|X} [g(Y) | X = \cdot] \in \mathbb{H}_X \forall g \in \mathbb{H}_Y$, then $\mathcal{C}_{XX} \mathbb{E}_{Y|X} [g(Y) | X = \cdot] = \mathcal{C}_{XY} g$, see [Fukumizu et al., 2004].*

Definition C.4. *Conditional Mean Embedding [Song et al., 2009].* Assuming that Proposition C.3 holds, then the CME of $\mathbb{P}_{(Y|X=\cdot)}$ is the operator $\mathcal{C}_{Y|X} : \mathbb{H}_X \rightarrow \mathbb{H}_Y$, whereas the evaluation of the conditional distribution $\mathbb{P}_{Y|\mathbf{x}}$ corresponds to the element $\mu_{Y|\mathbf{x}} \in \mathbb{H}_Y$:

$$\begin{aligned}\mathcal{C}_{Y|X} &:= \mathcal{C}_{YX} \mathcal{C}_{XX}^{-1}, \\ \mu_{Y|\mathbf{x}} &:= \mathcal{C}_{Y|X} \varphi_X(\mathbf{x}).\end{aligned}$$

From the reproducing property it follows that

$$\begin{aligned}\mathbb{E}_{Y|\mathbf{x}} [g(Y) | X = \mathbf{x}] &= \langle \mathcal{C}_{XX}^{-1} \mathcal{C}_{XY} g, \varphi_X(\mathbf{x}) \rangle_{\mathbb{H}_X} \\ &= \langle g, \mu_{Y|\mathbf{x}} \rangle_{\mathbb{H}_Y} \forall g \in \mathbb{H}_Y.\end{aligned}\tag{C.2}$$

The condition $\mathbb{E}_{Y|X} [g(Y) | X = \cdot] \in \mathbb{H}_X \forall g \in \mathbb{H}_Y$, will always hold for finite domains with characteristic kernels, but may not be valid for a continuous domain [Fukumizu et al., 2013]. A common approach to extend the condition to other systems is to consider the regularized inverse $(\mathcal{C}_{XX} + \varepsilon \mathcal{I})^{-1}$, where \mathcal{I} is the identity operator on \mathbb{H}_X , and $\varepsilon > 0$ is a Tikhonov regularization parameter [Tikhonov, 1977]. Moreover, \mathcal{C}_{XX} is a compact trace class operator, with eigenvalues that accumulate at zero when \mathbb{H}_X is infinite dimensional [Hsing and Eubank, 2015]. The regularization ensures a well-posed inverse.

All that is missing from the framework are the estimators for the CME. The empirical estimator of $\mathcal{C}_{Y|X}$ is given by,

$$\begin{aligned}\hat{\mathcal{C}}_{Y|X} &= \hat{\mathcal{C}}_{YX} (\hat{\mathcal{C}}_{XX} + \varepsilon \mathcal{I})^{-1} \\ &= \frac{1}{N} \Phi_Y \Phi_X^\top \left(\frac{1}{N} \Phi_X \Phi_X^\top + \varepsilon \mathcal{I} \right)^{-1} \\ &= \Phi_Y (\mathbf{K}_{XX} + N\varepsilon \mathbf{I}_N)^{-1} \Phi_X^\top \\ &= \Phi_Y \tilde{\mathbf{K}}_{XX}^{-1} \Phi_X^\top.\end{aligned}$$

Note that we can rescale the Tikhonov parameter $\varepsilon := \sigma_Y^2/N$, to coincide with the Bayesian interpretation and notation used in Appendix A.

The empirical estimator of $\mu_{Y|\mathbf{x}}$ permits the intuitive description as a weighted sum of dictionary elements Φ_Y , where the weights are dependent on the data point in \mathbb{X} on which we are conditioning. This line of reasoning leads us to

$$\hat{\mu}_{Y|\mathbf{x}} := \sum_{i=1}^N \varphi_Y(\mathbf{y}_i) \alpha_i(\mathbf{x}) = \Phi_Y \boldsymbol{\alpha}(\mathbf{x}),$$

where the weight vector is

$$\boldsymbol{\alpha}(\mathbf{x}) := \tilde{\mathbf{K}}_{XX}^{-1} \mathbf{k}_X(\mathbf{x}) \in \mathbb{R}^N.$$

Now the resemblance between (C.2) and (A.2) should be apparent. Moreover, it is easy to see that the CME coincides with the expression for the embedded PFO found in (2.3) when the input and output feature spaces are equal, i.e., $\mathbb{H}_X = \mathbb{H}_Y$.

Appendix D Estimation Algorithm

Here we detail a time-lagged canonical correlation analysis (TCCA) algorithm to yield a GP-DMD model. The algorithm is a variant of the algorithm in [Wu and Noé, 2020, Bach and Jordan, 2002], to which interested readers are referred for a more thorough theoretical discussion.

TCCA is a multivariate statistical method applicable to two sets of ‘featurized’ variables that are related by the flow map of a dynamical process. The algorithm is especially attractive, because it performs a decomposition that is similar to DMD, but with a valid interpretation for both reversible and *irreversible* processes, and for stationary and *non-stationary* processes. It finds a pair of linear orthonormal transformations – one for each set – such that the resulting projections are maximally correlated in time. The Koopman matrix can then be expressed in terms of these two transformations.

1. Using the transformation $\Psi_Z(\cdot) := \mathbf{L}_{ZZ}^{-1} \mathbf{k}_Z(\cdot)$ start by preconditioning the cross-covariance matrices:

$$\begin{aligned}\Psi_{ZX} &:= \mathbf{L}_{ZZ}^{-1} \mathbf{K}_{ZX}, \\ \Psi_{ZY} &:= \mathbf{L}_{ZZ}^{-1} \mathbf{K}_{ZY}.\end{aligned}$$

The lower triangular matrix \mathbf{L}_{ZZ} is obtained from the *Cholesky decomposition* of $\mathbf{K}_{ZZ} + \sigma_Z^2 \mathbf{I}_M$. This step simplifies upcoming computations, because the regularized Gramian matrix factorizes according to

$$\tilde{\mathbf{C}}_{XX} = \mathbf{L}_{ZZ} (\Psi_{ZX} \Psi_{ZX}^\top + \sigma_Y^2 \mathbf{I}) \mathbf{L}_{ZZ}^\top.$$

2. In this basis construct the $M \times M$ Gramian and stiffness matrices:

$$\begin{aligned}\mathbf{G}_{XX} &:= \Psi_{ZX} \Psi_{ZX}^\top, \\ \mathbf{G}_{YY} &:= \Psi_{ZY} \Psi_{ZY}^\top, \\ \mathbf{G}_{XY} &:= \Psi_{ZX} \Psi_{ZY}^\top.\end{aligned}$$

3. Proceed by performing (truncated) singular value decompositions (SVD) on the preconditioned covariance matrices:

$$\begin{aligned}\Psi_{ZX} &\approx \mathbf{M}_X \Sigma_X \mathbf{H}_X^\top, \\ \Psi_{ZY} &\approx \mathbf{M}_Y \Sigma_Y \mathbf{H}_Y^\top.\end{aligned}$$

4. Now we can include regularization by simply adding the noise variances to each of the principal variances:

$$\tilde{\Sigma}_{X,i} = \sqrt{\Sigma_{X,i}^2 + \sigma_Y^2}.$$

This implies that the inverse and inverse square root of the (noisy) Gramian matrices

can be expressed as

$$\begin{aligned}\tilde{\mathbf{G}}_{XX}^{-1} &= \mathbf{M}_X \tilde{\Sigma}_X^{-2} \mathbf{M}_X^\top, \\ \mathbf{G}_{YY}^{-1/2} &= \mathbf{M}_Y \Sigma_Y^{-1} \mathbf{M}_Y^\top.\end{aligned}$$

5. After normalizing the preconditioned cross-covariance matrices with $\tilde{\mathbf{G}}_{XX}^{-1/2}$ and $\tilde{\mathbf{G}}_{YY}^{-1/2}$, the half-whitened Koopman matrix can be computed with

$$\mathbf{U}' = \tilde{\mathbf{G}}_{XX}^{-1/2} \mathbf{G}_{XY} \tilde{\mathbf{G}}_{YY}^{-1/2},$$

which has the SVD:

$$\mathbf{U}' \approx \mathbf{W}'_X \mathbf{P} \mathbf{W}'_Y{}^\top.$$

6. Compute the transformation matrices:

$$\mathbf{W}_X = \tilde{\mathbf{G}}_{XX}^{-1/2} \mathbf{W}'_X, \quad \mathbf{W}_Y = \tilde{\mathbf{G}}_{YY}^{-1/2} \mathbf{W}'_Y.$$

7. Since the Markov model decomposes according to

$$\begin{aligned}\mathbb{E} [\mathbf{W}_Y^\top \Psi_Z(Y)] &= \mathbf{P} \mathbb{E} [\mathbf{W}_X^\top \Psi_Z(X)], \\ \mathbb{E} [\Psi_Z(Y)] &= (\mathbf{W}_X \mathbf{P} \mathbf{W}_Y^{-1})^\top \mathbb{E} [\Psi_Z(X)] \\ &= \mathbf{U}^\top \mathbb{E} [\Psi_Z(X)],\end{aligned}$$

the final Koopman matrix in the preconditioned basis is

$$\mathbf{U} = \mathbf{W}_X \mathbf{P} \mathbf{W}_Y^\top \tilde{\mathbf{G}}_{YY}.$$

8. The eigenvalue decomposition of \mathbf{U} will return \mathbf{V}_κ , and the modes with respect to the full-state observable are

$$\mathbf{V}_f = \Lambda^{-1} \mathbf{V}_\kappa \tilde{\mathbf{G}}_{XX}^{-1} \Psi_{ZX} \mathbf{Y}^\top.$$

D.1 Further Remarks

- (i) **Cholesky preconditioning.** Similar to [Baddoo et al., 2022], the Cholesky preconditioning step was also quite beneficial for numerical stability. As a bonus, due to the lower triangular structure of \mathbf{L}_{ZZ} the preconditioned matrices are efficiently found by solving the systems of linear equations.
- (ii) **Jitter term and noisy pseudo-outputs.** The jitter term, σ_Z^2 , may be regarded as another variational hyperparameter that we can optimize, and implies that the pseudo-outputs \mathbf{f}_Z are noisy.
- (iii) **TCCA interpretation and Koopman singular functions.** As mentioned, TCCA provides another set of quantities by which we can analyze and interpret the dynamical system. The left and right *singular functions* of the Koopman operator are respectively approximated by $\mathbf{W}_X^\top \Psi_Z(\cdot)$ and $\mathbf{W}_Y^\top \Psi_Z(\cdot)$, and can be used to identify *coherent sets* [Froyland et al., 2010, Klus et al., 2019].

The goal of TCCA is to simultaneously transform $\Psi_Z(X)$ and $\Psi_Z(Y)$ in such a way that the cross-correlation between the whitened vectors are diagonal. More formally, the first *canonical correlation* is defined by the optimization problem in primal form:

$$\begin{aligned} \rho_1 &= \max_{\mathbf{w}_X, \mathbf{w}_Y} \frac{\text{cov}(\mathbf{w}_X^\top \Psi_Z(X), \mathbf{w}_Y^\top \Psi_Z(Y))}{\sqrt{\text{var}(\mathbf{w}_X^\top \Psi_Z(X)) \text{var}(\mathbf{w}_Y^\top \Psi_Z(Y))}} \\ &= \max_{\mathbf{w}_X, \mathbf{w}_Y} \text{corr}(\mathbf{w}_X^\top \Psi_Z(X), \mathbf{w}_Y^\top \Psi_Z(Y)), \end{aligned}$$

subject to constraining the images to unit variance

$$\begin{aligned} \text{var}(\mathbf{w}_X^\top \Psi_Z(X)) &= 1 \approx (1/N) \mathbf{w}_X^\top \tilde{\mathbf{G}}_{XX} \mathbf{w}_X, \\ \text{var}(\mathbf{w}_Y^\top \Psi_Z(Y)) &= 1 \approx (1/N) \mathbf{w}_Y^\top \tilde{\mathbf{G}}_{YY} \mathbf{w}_Y. \end{aligned}$$

The problem is then generalized to finding an ordered list of correlations, which we package into the diagonal matrix \mathbf{P} , along with the associated transformations \mathbf{W}_X and \mathbf{W}_Y .

- (iv) **Hyperparameter selection via VAMP score.** As we demonstrated in Section 3, choosing the hyperparameters can be accomplished with a *VAMP-score*, which is a metric that quantifies the similarity between the estimated singular functions and the true ones. An example is the squared sum of canonical correlations, i.e., the VAMP-2 score or the total *kinetic variance* [Noé and Clementi, 2015], which is a quantity that reaches its maximum when all the patterns extracted from the data are perfectly linear, i.e., $\rho_i = 1 \forall i \in [\min(\dim(\Sigma_X), \dim(\Sigma_Y))]$.

Appendix E The Bayesian-consistency kernel

Since ν_i is an \mathbb{H} -valued Gaussian random element defined by the covariance operator \mathcal{C}_{bc} , i.e.,

$$\mathbb{E}[\langle \nu_i, g \rangle_{\mathbb{H}} \langle \nu_i, f \rangle_{\mathbb{H}}] = \langle g, \mathcal{C}_{bc} f \rangle_{\mathbb{H}} \quad \forall f, g \in \mathbb{H}.$$

Then the induced scalar process $\nu_i(\mathbf{x}) = \langle \nu_i, \varphi(\mathbf{x}) \rangle_{\mathbb{H}}$ is a Gaussian process associated with the Bayesian-consistency kernel, and can be related to the feature map of the prior covariance function:

$$\kappa_{bc}(\mathbf{x}, \mathbf{x}') = \langle \varphi(\mathbf{x}), \mathcal{C}_{bc} \varphi(\mathbf{x}') \rangle_{\mathbb{H}}.$$

Since $\mathbf{K}_{bc} := [\kappa_{bc}(\mathbf{z}_i, \mathbf{z}_j)]_{i,j=1}^M \in \mathbb{R}^{M \times M}$ it follows that

$$\mathbf{K}_{bc} = \Phi_Z^\top \mathcal{C}_{bc} \Phi_Z.$$

Given a finite-rank approximation of \mathcal{C}_{bc} supported on the span of Φ_Z , such that

$$\mathcal{C}_{bc} \approx \sum_{i,j=1}^M \mathbf{C}_{bc,ij} \varphi(\mathbf{z}_i) \otimes \varphi(\mathbf{z}_j) = \Phi_Z \mathbf{C}_{bc} \Phi_Z^\top, \quad \mathbf{C}_{bc} \in \mathbb{R}^{M \times M},$$

we obtain the expression

$$\mathbf{C}_{bc} = \mathbf{K}_{ZZ}^{-1} \mathbf{K}_{bc} \mathbf{K}_{ZZ}^{-1}.$$